Volume 2
№2, 2019

ISSN: 17184-Ж

MATERIAL AND MECHANICAL ENGINEERING TECHNOLOGY

Content

The Hybrid Fuel Cell Locomotive Concept

Mario Mišić
J. J. Strossmayer University of Osijek, Croatia

Abstract: The main idea arose as a modification of the original diesel locomotive. For environmental reasons, to save money and energy consumption, the paper describes some general fuel cell laws and their use in the vehicle. At the end of the paper energy saving and fuel economy are described. The focus is on the cost-effectiveness of the hybrid fuel cell concept. The main objective is the recognition of hydrogen and the cost-effectiveness of maintenance. The construction of a locomotive is based on a prototype, which can also be recognized as a limited economic aspect.

Keywords: fuel cell, fuel economy, hybrid vehicle, hybridization, diesel locomotive, hybrid locomotive, hydrogen.

1 Introduction

1.1 Fuel consumption

Main internal combustion (IC) engines problems are pollutants and greenhouse gases. Especially large diesel engines have increased pollution by particles and nitrous oxides. On another way, huge oil consumption in this decade and world demand for fossil fuels are increased and also high gasoline and oil prices are to stay. Resolving of problem could be in hybrid vehicles with fuel cells.

1.2 What is the fuel cell?

Fuel cells efficiently convert the chemical energy of a fuel into usable electrical energy through electrochemical reactions. Among the various types, polymer electrolyte fuel cells (PEFC) are attracting the most attention for automotive applications and small stationary applications because of their higher electrical efficiency, power density and durability. In a PEFC, hydrogen and oxygen are electrochemically combined in a solid polymer electrolyte to produce electricity, water and heat. The operation of a PEFC involves a complex overlap of interrelated physicochemical processes, including electrochemical reactions and the transport of ions, electrons, energy and species in gas and liquid phases by heterogeneous media. Although PEFCs have shown promising performance improvements in efficiency and durability over the past three decades [1].

2 Fuel cells

2.1 General about PEFCs

By combining hydrogen and oxygen into water through electrochemical reaction, a fuel cell will generate electricity. The chemical reaction is based on the catalytic combination of hydrogen with oxygen. The catalytic reaction releases electrical energy and pure water. In contrast to internal combustion engines or electric motors, fuel cells have no moving parts and they have a longer life. The amount that it can transport is limited.

A single fuel cell produces a very low voltage, usually less than 1 volt. To provide the power required to drive a vehicle, several hundred fuel cells are connected in series. This assembly is the fuel cell stack. This is referred to as a fuel cell stack because the cells are juxtaposed or stacked. Each fuel cell produces electricity and the combined power of the cells is used to power the vehicle.

A fuel cell has two electrodes coated with a catalyst. The electrodes are separated by an electrolyte and separators. The anode has a positive polarity and the cathode has a negative polarity. The electrolyte is mostly a polymer membrane called a proton or ion exchange membrane. Polymer membrane is very resistant to chemicals and is used as an electrical insulator and separator. The catalyst, usually platinum, on electrodes causes the chemical reaction in the fuel cell but does not significantly participate in the reaction. In a fuel cell, only hydrogen and oxygen are involved in the chemical reaction, not the catalyst. The oxygen is used from the air and directed into the cell by an air compressor. Hydrogen is fed from a pressure tank into the fuel cell.

When hydrogen is supplied to the anode, the catalyst causes the hydrogen atoms to separate into electrons and protons. Electrons always move to something more positive, but they can't get through the membrane. Their only way to the positive side of the fuel cell therefore leads via an external circuit. The movement of electrons through this circuit leads to a direct current flow. This current flow drives the electric drive motors of the vehicle.

Oxygen penetrates to the other side of the fuel cell and reacts to the catalyst at the cathode. This reaction divides the oxygen molecules into oxygen ions. The hydrogen ions released from the anode at the anode move in direction of the oxygen ions. The membrane separates two electrodes and allows only protons to pass and they do. At the cathode, two hydrogen ions combine with each oxygen ion to form water. To function, the ion exchange membrane must be kept moist. Therefore, part of the water generated by the fuel cell is used to humidify the incoming hydrogen and oxygen. The remaining water is discharged as exhaust gas from the fuel cell. Some heat is also given off by the fuel cell. The heat is either released to heat the passenger compartment.

2.2 Chemical reaction

PEFC at temperatures where certain oxide electrolytes become oxygen ions O^{2-} conductive. The two electrode reactions are expressed as [2]:

- chemical reaction at the anode: $H_2 \rightarrow 2H^+ + 2e^-$
- chemical reaction at the cathode: $O_2 + 4e^- + 4H^+ \rightarrow 2H_2O$

A PEFC converts the intrinsic chemical energy of a fuel into electrical and heat energies. Usually, the fuel cell is operated at a temperature greater than the standard temperature of 25 °C. This needs to be accounted for when estimating the thermodynamic properties of the system. Depending on if the product water is vapor or liquid, one arrives at different potentials due to the latent heat and free energy difference between liquid and vapor water. Thus, as the cell temperature increases, the amount of usable work from the fuel decreases, while the amount of heat generated increases for a given operating potential.

3 The hybrid fuel cell locomotive

3.1 Diesel locomotive

As is known, the total resistance forces of vehicle driving are rolling resistance, aerodynamic drag, acceleration and climbing force (Figure 1). Empirical formulas (Davis equations) for driving freight wagons are described by a mathematical model of total drag forces [3]:

$$R_h = 1300 + 10v + 0.03v^2 \ [\text{kN}] \tag{1}$$

where v is speed of locomotive in km/h.

The total weight of the locomotive is 72 000 kg, the weight of the pulled freight train is about 1000 tons and traction power is 600 kW. The traction force is divided into two segments by the critical speed at 10 km/h. The first segment is described as a mathematical friction model [4]:

$$F_{tr1} = m_L \cdot g \cdot (0.161 + \frac{7.5}{v + 44})[\text{kN}] \tag{2}$$

where v is speed of locomotive in km/h;

m_L is mass of locomotive in tones;

g is gravitational acceleration in m/s^2.

The second segment is described as a mathematical power model:

$$F_{tr2} = \frac{P}{v} \ [\text{kN}] \tag{3}$$

The main engine components for diesel locomotives are the Caterpillar 3508C engine, the main generator and the fuel tank. These components are not installed in hybrid locomotives (Table 1). All these elements are important for the energy consideration.

Table 1 - Masses of main components

Component	Mass [kg]
Locomotive	72000
Diesel engine CAT 3508C	4580
Main generator	2200
Fuel tank	4250

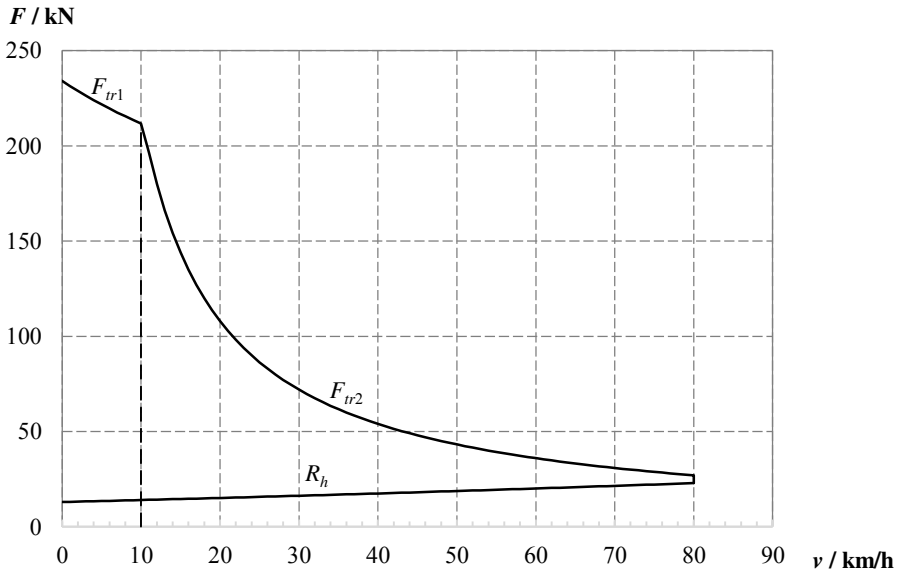

Fig. 1 - Diesel locomotive traction characteristics

3.2 Energy Considerations

Minimizing energy consumption is often a popular focus in train management. It is helpful to examine how energy is used before innovations or changes are made in practice. According to the Davis equation, the importance of air resistance is superior to curvature, rolling resistance factors and degree.

The minimum energy required for a ride can be estimated by assuming an average train speed and calculating the sum of the motion resistances, not forgetting the possible energy effects of altitude changes. The work that is done to get the train up to speed once must be added. Since the train has to stop at least once, this energy is lost at least once. The minimum impact energy can be estimated as [3]:

$$E_{\min} = \frac{1}{2} m_t v^2 + m_t g h + \sum_{j=1}^{q} m_i \int_0^{x=L} R_h \mathrm{d}x \tag{4}$$

where g is gravitational acceleration in m/s^2;
h is the track altitude change in m;
L is the track route length in m;
m_i is individual vehicle mass in kg;
m_t is the total train mass in kg;
R_h is the propulsion resistance for vehicle i in N;
q is the number of vehicles;
v is speed of train in m/s.

3.3 Compressed hydrogen

The need for easier gas storage has led to the development of lightweight composite cylinders instead of steel. Conventional carbon-wrapped aluminum cylinders can store hydrogen at a pressure of 55 MPa (550 bar). Gas cylinders are normally filled up to 30 MPa (300 bar). Hydrogen storage may also require the use of a polymer barrier to reduce gas permeability.

Today it is possible to produce a cylinder volume of 140 liters (65 kg) at a pressure of 34.5 MPa (345 bar). These cylinders supply the fuel cell with approx. 2.9 kg of hydrogen. The critical temperature of hydrogen, under which the gas can be liquefied, is 33 K (table 2) [5].

Table 2 - Compressed hydrogen parameters

Parameter	Value
Boiling point [K]	33
Lower heating value [MJ/kg]	121
Specific energy (Wh/kg) [MJ/kg]	2630
Density [kg/m^3]	70

Fuel consumption per hour is:

$$\dot{m}_{F,h} = g_e \cdot P_e \left[\frac{\text{kg}}{\text{h}}\right] \tag{5}$$

where g_e is specific effective fuel consumption in kg/kWh;
P_e is effective power in kW.

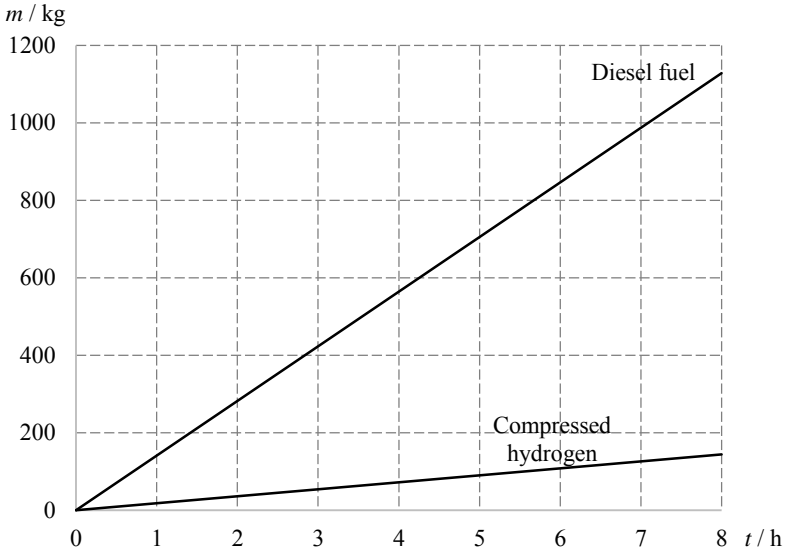

Fig. 2 - Comparison of fuel consumption

As noted (Figure 2), for a 600 kW locomotive operating at 8 hours, the diesel consumption should be approximately 1120 kg. The consumption of compressed hydrogen should be about 150 kg. Zero-emission vehicles, as hybrid fuel cell locomotives, have good prospects for low fuel prices.

Table 3 - Hydrogen tank parameters

Parameter	Value
Diameter [mm]	280
Length [mm]	2360
Volume [L]	140
Mass [kg]	65
Service Pressure [bar]	345
Burst Pressure (minimum) [bar]	776
Hydrogen Contained [kg]	2.9
Quantity of Tanks	50

3.4 A hybrid fuel cell locomotive system

A hybrid fuel cell system consists of a fuel supply system, an air supply system, a water management system, a fuel cooling system, an battery, an inverter, an inverter for the rheostat chopper and 3-phase traction motors (Figure 3). A hybrid energy locomotive system uses DC power of a fuel cell with battery hybridization. The DC voltage is converted to 2.8 kV and the traction converter is switched to 3-phase AC before being fed to the traction motors. The traction motors can also serve as generators and the recycled energy is used to charge the batteries. The regeneration braking power control is performed by using a bidirectional DC/AC power semiconductor operating in the rectifier mode. In braking mode, the controller is routed from the power source to energy storage batteries (Figure 4).

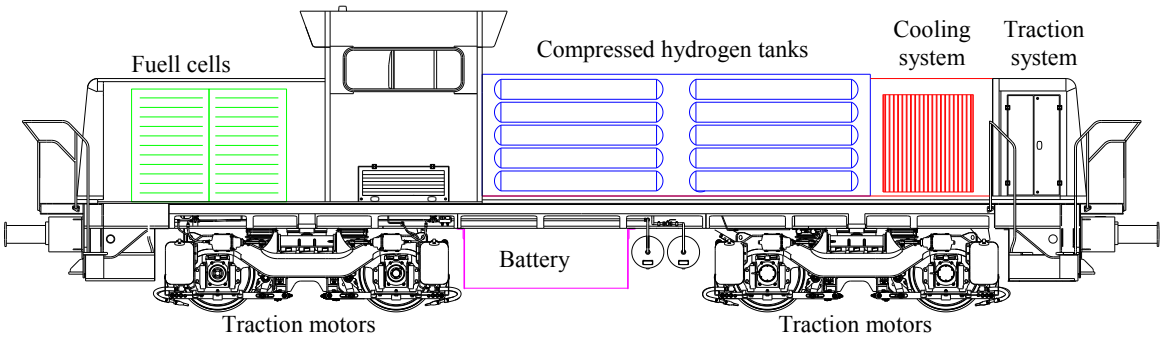

Fig. 3 - The hybrid fuel cell locomotive configuration

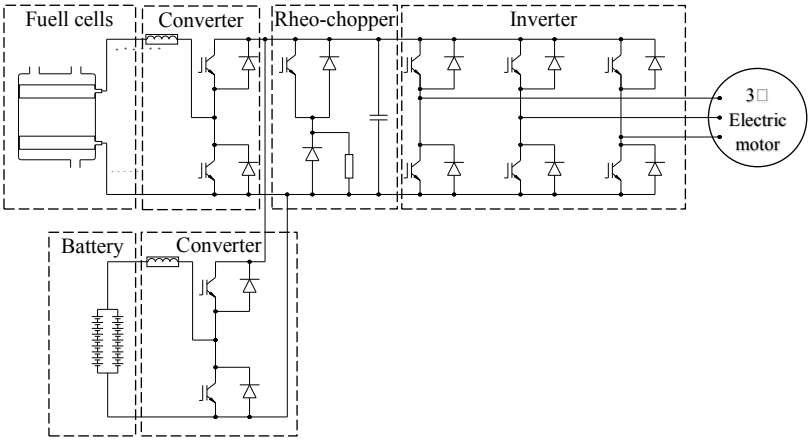

Fig. 4 - The hybrid fuel cell locomotive traction system

The main purpose of the locomotive is maneuvering. The locomotive consists of a fuel cell block of 400 kW and a battery of 240 kW. The traction uses 500 kW, the remaining power is used as a reserve and to supply additional equipment. Battery is also used as a regenerative brake energy storage and as a main energy supplier when the fuel cell system operates at low load.

Table 4 - Weights of main components

Component	Mass [kg]
Locomotive	71000
Fuel cell	2900
Compressed hydrogen tanks	3400
Battery	4000

4 Analysis of energy usage

4.1 Average cost of fuel cell locomotive

The fuel consumption depends on the hybridization ratio. The hybridization ratio is defined as [6]:

$$HR = \frac{P_{batt}}{P_{tot}} \tag{6}$$

where P_{tot} is total power of hybrid vehicle;

P_{batt} is power of installed battery.

With a battery price of 365 €/kW, the total price of the vehicle is determined by a different hybridization ratio (table 5). At an average fuel cell price of 600 €/kW, the price of locomotive shouldn't be higher than 1 mil. €.

Table 5 - Price of main components

Component	Price [€]
Car body	400000
Battery	91250
Compressed hydrogen tanks	10000
Fuel cell	240000
Traction system	120000
Cooling system	50000
Total	911250

For this vehicle, hybridization ratio is:

$$HR = \frac{240}{600} = 0.4 \tag{7}$$

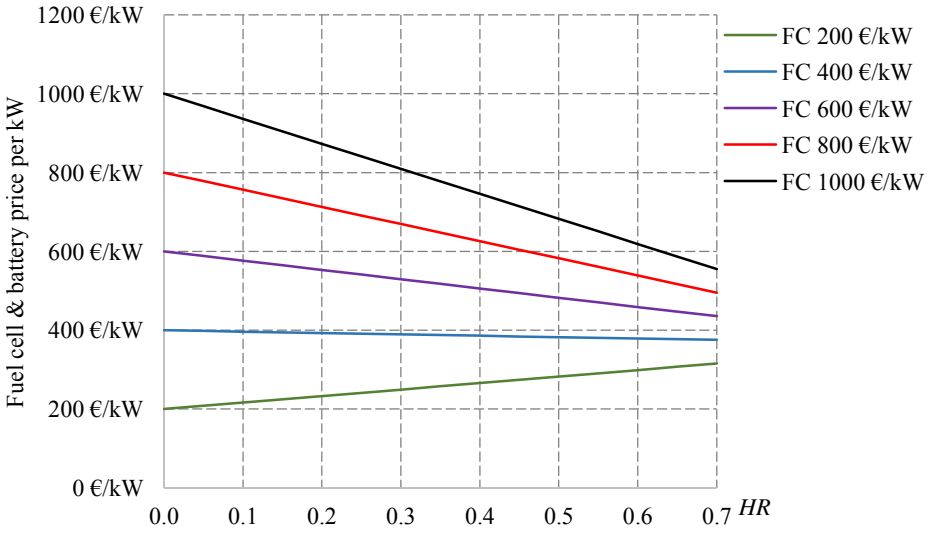

Fig. 5 - Fuel cell (FC) economy for different hybridization ratio and fixed battery price of 365 €/kW

4.2 A fuel economy

With a higher hybridization ratio, fuel consumption is more efficient. Hydrogen prices are between 10 €/kg and 20 €/kg and diesel fuel between 1.5 €/kg and 2.5 €/kg in the last three years (fig. 6). When the hybridization ratio is more than 0.33, the fuel consumption decreases. With a hybridization ratio of 0.33, the charge and discharge time of the battery is higher and the battery can be used longer than the main drive.

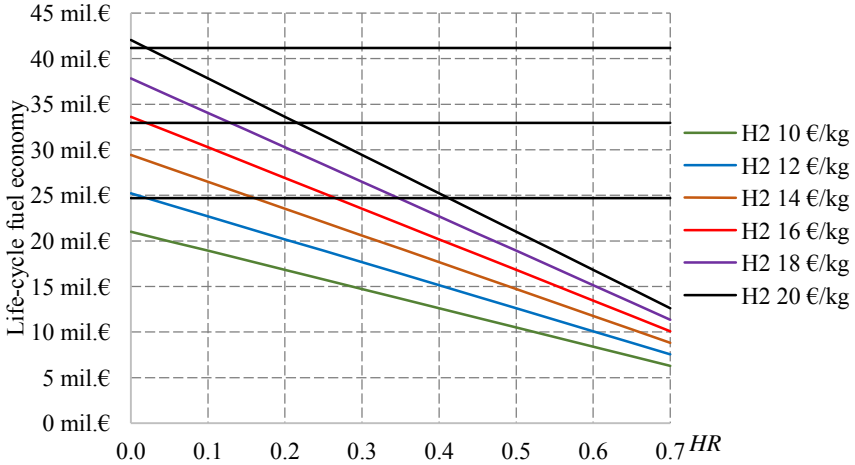

Fig. 6 - Fuel economy for locomotive life-cycle

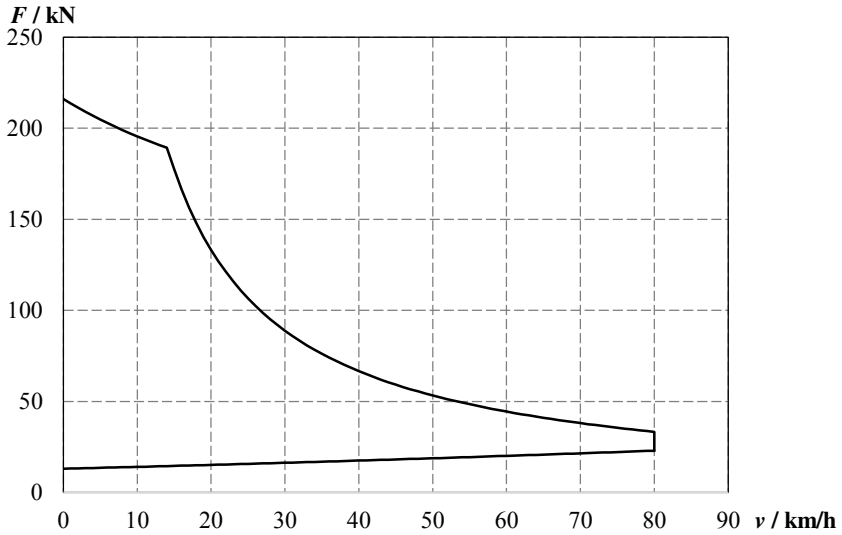

Fig. 7 - The hybrid fuel cell locomotive traction characteristics

4.3 Life-cycle cost

In 40 years of the locomotive's life cycle, there are many important maintenance factors. First, there is no life cycle battery for more than 10 years. In general, the energy capacity of the battery fades over time and over the discharge cycles. With a state of charge (SOC) consumption of 70%, a lithium-ion battery can typically last 4000 charge cycles. That's about 10 years. After this time, the battery capacity can only be 50% of the original capacity. The battery should be changed every 10 years.

As the degree of hybridization increases, life cycle costs decrease. Vehicles with more powerful fuel cells and higher levels of hybridization reduce manufacturing costs and life-cycle costs.

5 Conclusion

With a higher hybridization ratio, life-cycle costs and fuel consumption are very reasonable. In accordance with environmental and environmental standards, this is an emission-free vehicle. The main problems are hydrogen liquefaction and battery life. Hydrogen liquefaction can be done in two ways: reducing the temperature to 33 K, which causes 40% energy loss, or pressurizing to 345 bar, causing 13% energy loss. In any case, however, energy losses are unavoidable and the price of hydrogen per 1 kg could be lower by increasing production.

The battery life is much longer than it was 10 years ago. For future improvements, the life cycle should be as long as possible. The main goal is to avoid battery replacement after ten years.

Technological conditions are still not fulfilled before the fuel cell power system can justify installation, performance and reliability costs. For a successful commercialization of fuel cell vehicles, the market has to open up and go into larger serial production to survive. Fuel cell research will provide improvements in performance and cost. Clearly, fuel cells can be adopted as a cleaner and more efficient drive. Scientific contribution is a demonstration that a hybrid vehicle with fuel cells can be built with relatively low costs, but if the industry does not understand, there will be no shift.

References

[1] Weber A., Das P., and Balasubramanian S., Advances in Chemical Engineering, Fuel Cell Engineering, Academic Press, Volume 41, Berkeley, USA, 2012.

[2] Kuang K., Easler K., Fuel Cell Electronics Packaging, Springer Science + Business Media, New York, NY, USA, 2007.

[3] Iwnicki S., Handbook of railway vehicle dynamics, Taylor & Francis Group, Boca Raton, FL, USA, 2006.

[4] Ihme J., Schienenfahrzeugtechnik, Springer Fachmedien, Wiesbaden, Germany, 2016.

[5] Mitlitsky F., Weisberg A., Myers B., Conference: U.S. DOE Hydrogen Program 2000 Annual Review Meeting, San Ramon, CA, USA: U.S. Department of Energy, 05/09/2000-05/11/2000.

[6] Seong Jeong K., Soo Oh B., Fuel economy and life-cycle cost analysis of a fuel cell hybrid vehicle, Journal of Power Sources 105 (2002) 58–65, Amsterdam, Netherlands, 2002.

Innovation Methods of Manufacturing High-Strength Shell Molds in Foundry Production

Kulikov V.Yu., Issagulov A.Z., Kvon Sv.S., Kovaleva T.V.
Karaganda State Technical University, Kazakhstan

Abstract: The article deals with obtaining sand-resin molds using static loads. Based on the studies carried out, a molding machine and technology for manufacturing shell molds for mining equipment castings have been developed, tested in industrial conditions and proposed for use.

Keywords: sand-resin mixture, shell form, strength, density, gas penetration, roughness.

1. Introduction

One of the representatives of dispersion media is a sand-resin mixture. Such mixtures are widely used in practice in metallurgy and foundry [1 - 4]. Building mathematical models of mixtures and compaction processes to describe the stress-strain state is carried out in order to select rational schemes and compaction modes, and allows controlling the structure of molds. As a result, it is possible to control the mold properties, such as density, gas permeability.

In this regard, studies aimed at improving technological processes in the metallurgy and foundry industry, in particular, obtaining durable and dense sand-resin molds with decreasing the content of the binder in the mixture, without worsening other parameters, is relevant.

Increasing the shell molds strength will reduce the binder consumption [5 - 8]. At this, attention should be paid to ensuring no other mechanical and technological indicators of the shell mold decreasing.

Reducing the resin consumption for manufacturing shell molds will reduce the cost of producing molds.

It is also known that pressing allows increasing the speed of molding and improving the quality of the shell [9 - 12]. Pressing increases the strength of both clad and unclad mixtures. For practical purposes, it is recommended to apply the pressing force up to 0.2 MPa [13 - 16].

Compaction of the sand-resin mixture when shaping shell molds has a positive effect on reducing mold rejects and on increasing the rate of shell molding. That is, it allows eliminating the above disadvantages. In addition, pressing increases strength and is applicable for clad and unclad mixtures, which will reduce the binder content in the mixture and, accordingly, the cost of molds.

It is possible to achieve a greater increase in strength of the shell mold at the expense of slight increasing pressure from the initial one (that is, pressure in the time of molding the shell changes). As a rule, the whole cycle of shell mold shaping on a model plate lasts within 30 s. It is necessary to increase initial pressure that is 0.18...0.25 MPa, by 0.03...0.05 MPa, and this should be done within 5...10 s after the start of filling the sand-resin mixture onto the heated plate. The pressing can be carried out by a diaphragm or a pressing plate. Increasing the pressure at some later time leads to violating the mold shell in the mixture layer adjacent to the heated model plate. Due to increasing pressure in the process of molding, the packing density of the filler grains (sand) and the adhesive properties of the resin increase, due to a more uniform and complete enveloping of the sand grains (melting resin binds the sand grains more firmly). At this, the remaining technological indicators of the mold (gas permeability, roughness) remain within the limits of the needed.

The rate of the shell molding increases when using pressure on the mixture in the process of shaping. When using a press plate for compacting the mixture, it is possible to feed the mixture directly to the model plate through openings in the plate, for example, with a slide gate. At this, the mixture will be supplied to the model plate in the perpendicular direction. Manufacturing shell molds is carried out by applying the sand-resin mixture to the model mounted on the model plate. In this case, the mixture is fed simultaneously to all parts of the model surface and is distributed evenly with simultaneous compaction and obtaining the layer of a constant thickness.

A device for manufacturing shell molds includes a model plate, a model fixed on the model plate and a device for feeding the sand-resin mixture to the surface of the model. It is a container with outer and inner side walls, the top wall and the bottom; the inner side wall has the shape of an enlarged model to form a gap between the wall and the real model, and there are through holes for feeding the mixture, with a slide gate; the upper wall has a window for filling the container with the mixture connected with the facility for applying pressure in the cavity of the container, and the bottom is made of an elastic material which supporting surface is reinforced with a metal plate. It is also necessary to foresee a gap between the pressing block and the model plate. The gap must be equal to the thickness of the shell mold and be determined in advance (Figure 1).

Sand-resin mixture 2 is fed through opening 1 into the internal cavity of the pressing plate. After feeding the pressure head to the model plate the gates are opened and the mixture is fed to model plate 4 and model 5. At this the mixture volume is limited by the gap between the pressure head and the model. Thus there is achieved the dosing accuracy. In order to be able to adjust the size of the gap, as well as to compact the mixture, the bottom of the pressure head should be made of elastic material 6, for example, rubber that is protected from heating and melting with metal plate 7. The mixture on the model plate, the gates close the holes. Subsequently, the mixture is compacted by increasing pressure on the plate, which, due to the compression of the head portion made of an elastic material, presses against the mixture.

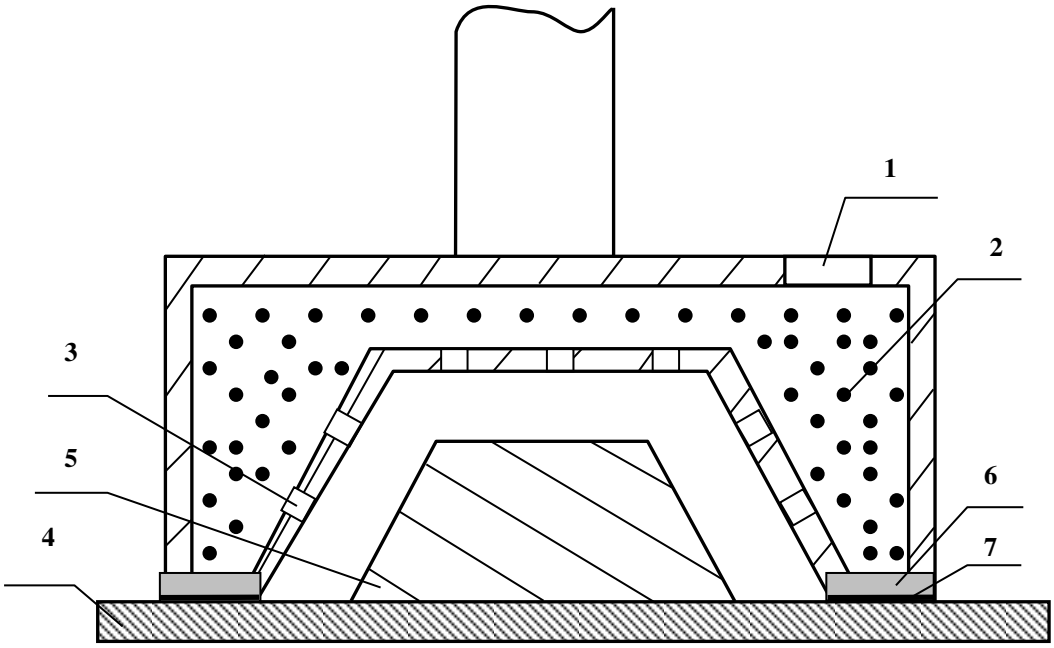

Fig. 1 – A device for manufacturing shell molds

However, in case of using rigid plate walls, this device can only be used in tandem with a particular model, that is, a specific plate should be used for each model. Changeover requires time and material costs.

In addition, it is possible to overrun the mixture when it is jammed in the places where the surfaces mate, especially in models with complex configurations.

Besides, when using this method, it is necessary to provide in advance a gap between the pressing block and the model plate that should be equal to the thickness of the shell mold and be determined in advance.

When using the same membrane as a means of transmitting pressure to the mixture and feeding the mixture directly to the model plate through the openings in the pressing device of the plate, there is used, for example, a slide gate. In case of using an elastic membrane, the mixture will be supplied to the model plate in the direction perpendicular to the model itself, which will increase the shell being mold, especially in the part adjacent to the model. The production of shell molds is carried out in the same way as in the previous case by applying the sand-resin mixture to the model fixed on the heated model plate. In this case, the mixture is fed through the membrane wall of the press simultaneously to all parts of the model surface strictly perpendicular to the model with simultaneous compaction.

To increase the rate of the mixture feeding to the model plate and the degree of compaction, pressure of 3...5 at. is formed in the cavity of the pressure head through opening 1, and the mixture fall on the plate with the speed of 1-2 m/s.

Thus, the use of such a method and device for feeding the sand-resin mixture to the model and the model plate will provide the following:

1. Reducing the time for manufacturing shell half-molds due to the combination of the process of filling and compacting the mixture, no need to pour out the excess mixture.
2. The accuracy of dosing the mixture consumed for manufacturing shell half-molds.
3. A uniform layer thickness throughout the shell due to the uniform mixture feed to the surface of the model plate.
4. The ability to use both clad and unclad mixtures.
5. The absence of dust emission when manufacturing shell half-molds.
6. No need to use a frame (flask) to hold the mixture in the process of shell shaping.

2. Results and discussion

An experimental set for manufacturing shell molds of a sand-resin mixture (Figure 2) is made on the basis of the 51713 model of a semi-automatic molding machine and consists of a hopper in which the sand-resin mixture is poured, an oven, plates for additional static load application, a table on which an electrically heated model plate with the model is mounted. A filling frame is mounted on the model plate.

Fig. 2 – An experimental set

On the model plate there were mounted radiator models, on the back side of which there were spring pushers (in order to separate the finished shell half-molds from the model) and electric heaters. A thermal sensor was also located there, with the help of which the heating of the plate was controlled to 240-260 ^{0}C.

A filling frame (flask) with the height of 100 mm along the perimeter coinciding with the hopper was mounted on the model. In the initial position the models were covered with a drying oven casing. Nearby a hopper was located, in which the mechanical mixture of sand with pulverbakelite and some additives was poured. The machine can operate in both automatic and manual modes.

Before the work the model plate was covered with a parting compound, for which a mixture of water 100%, household soap 3%, PMS (silicone) 8% were used. At the time of applying to the hot model, the parting compound forms a thin and hard but heat-resistant film that is preserved after several shells are removed from the models.

When turning on the molding machine, the oven rose up, and the mixture was filled from the hopper to the model plate. At the same time on the filling frame with the poured mixture the plate was lowered, exerting a static load on the mixture. Then the plate was returned to its original position.

Under the action of the heat of model equipment, pulverbakelite melted and wetted grains of sand in the layer of the mixture immediately adjacent to the model plate.

After receiving the shell, the plate returned to its original position, and the models with the shell were covered with the oven, inside which the temperature was about 350 °C. Instead of gas nozzles on the oven there were mounted electric coils. The shell thickness was 8-12 mm.

The tensile and bending strength of the sand-resin mixtures were determined on standard samples (Figures 3-6). Strength testing devices are presented in Figures 7-9. Some parts of the shell experience dynamic pressure of the metal jet, the magnitude of which is proportional to the velocity and cross-sectional area of the jet. The remaining parts of the mold perceive the metal static pressure.

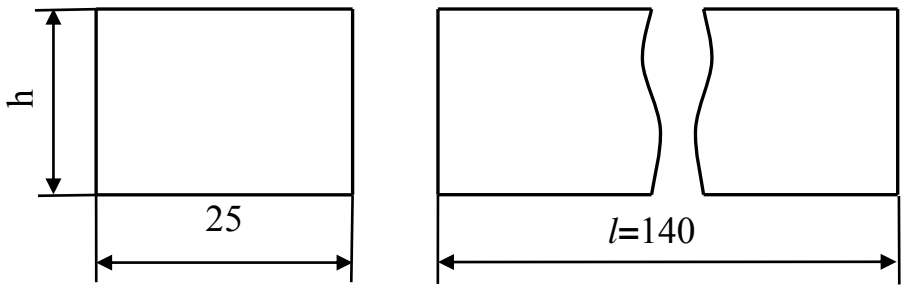

Fig. 3 – Shapes and sizes of the samples for bending testing

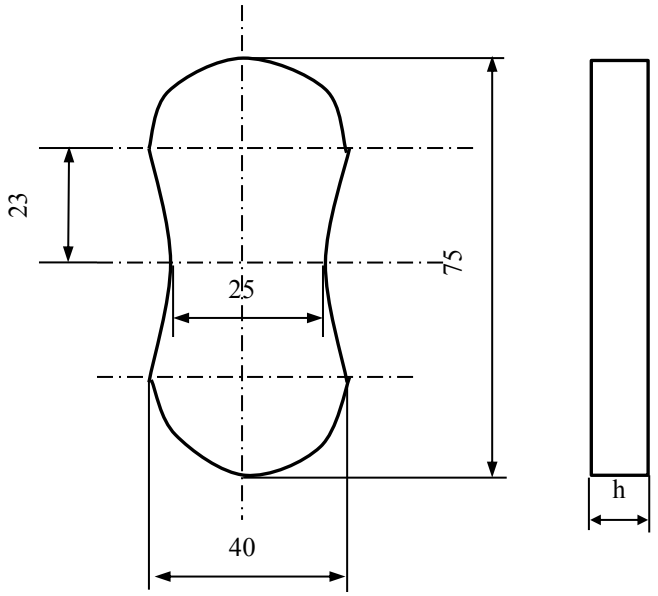

Fig.4 – Shapes and sizes of the samples for tensile testing

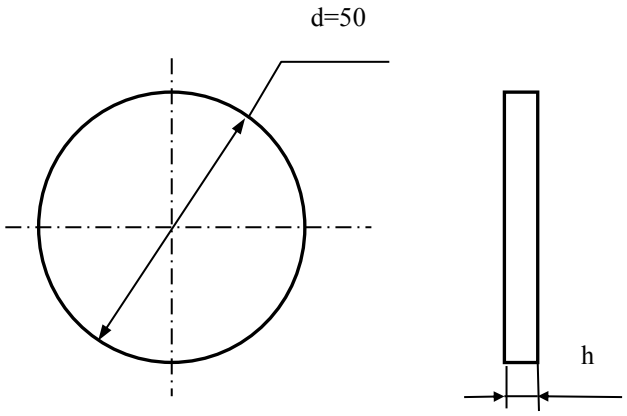

Fig.5 – Shapes and sizes of the samples for compressive testing

The samples were made in accordance with the manufacturing technology of shell molds. The samples for strength testing (Figure 6) were manufactured in the technological process similar to the process of manufacturing shell molds and cores. The thickness *h* of the samples depended on the pressure value, the degree of heating of the model plate, the exposure time on the plate, the thickness of the preliminary backfill of the sand-resin mixture. The strength index was considered the arithmetic average of the results. If the data of one sample differed from the arithmetic average by more than 10%, then the tests were repeated.

Gas permeability of the SRM was determined on the device for determining gas permeability 042 UZM. There were tested samples similar to the samples for determining compressive strength.

The molds and castings roughness was determined on the electronic device for measuring roughness TR-100.

In the experiments carried out the content of the binder (pulverbakelite) in the mixture varied from 1 to 7%. The shaping of the shell mold was accompanied by pressure applied to the mixture within the entire time of the shell shaping.

Fig. 6 – Samples for strength testing

Fig.7 – Facilities for making samples for strength testing

Fig.8 – A sample for determining tensile strength before the testing

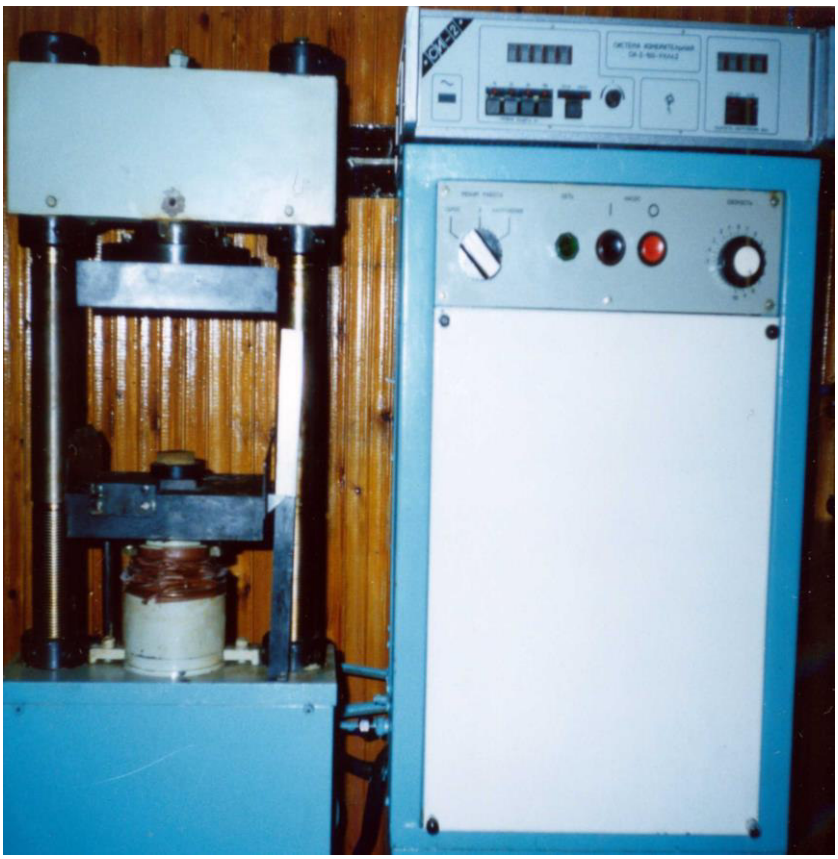

Fig. 9 – A press and a sample for testing compressive strength

Figure 10 shows the graph of the shell bending and breaking strength on the content of humidifier (kerosene) and binder (pulverbakelite).

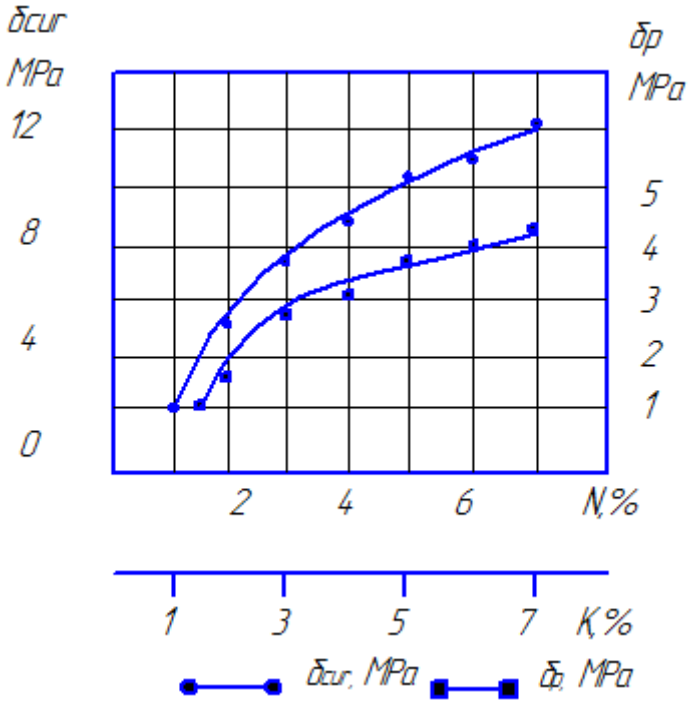

Fig. 10 – Shell molds bending and breaking strength dependence on the content of pulverbakelite and kerosene

With increasing the content of pulverbakelite in the mixture its strength characteristics increase due to increasing adhesion of the resin with sand particles. However, after exceeding 5-6% of the binder content, strength increases but slightly.

In another series of experiments the dependence of tensile strength and bending on the applied static pressure on the mixture when shaping the shell was determined. The pressure through the press plate was carried out with compressed air from the pipeline. A plot of tensile strength and bending versus the applied static pressure on the mixture is shown in Figures 11-12. It is experimentally determined (Table 1) that applying pressure to the mixture increases strength. With increasing pressure after 0.2–0.25 MPa, the strength increases, but the intensity of increasing strength decreases with increasing pressure. Thus, the optimum pressure when molding casings for heating equipment should be 0.18-0.25 MPa.

Table 1 – Tensile and bending strength dependence on applied static pressure in the course of the shell shaping

Experiment No.	Pulverbakelite content %	Pressure, MPa	σ_p, MPa	σ_{arc}, MPa	Note
1	5	0.1	3.8	9.1	Mechanical belnding of
2	5	0.2	4.3	11.4	pulverbakelite and sand.
3	5	0.3	4.5	12.5	The sand composition:
4	5	0.4	4.6	13.2	1K02 100%
5	5	0.5	4.7	13.3	
6	5	0.6	4.7	13.2	
7	5	0.7	4.8	13.9	
1	5	0.1	3.5	8.5	Mechanical belnding of
2	5	0.2	4.2	9.9	pulverbakelite and sand.
3	5	0.3	4.4	11.0	The sand composition:
4	5	0.4	4.5	12.0	1K016 100%
5	5	0.5	4.6	12.6	
6	5	0.6	4.7	12.8	
7	5	0.7	4.6	13.4	

Using one fraction sands in the mixture with increasing pressure leads to parallel increasing the mixture strength. When using mixed fractions, sands with a larger fraction initially have greater strength; when using pressures above 0.45 MPa the mixtures with a smaller fraction filler have a somewhat greater strength both at break and bending. This is due to the more complete removal of the inter-pore air and the fact that the smaller fractions sands are more dense ("monolithic") adjacent to each other at the given pressure, providing greater strength for the mixture.

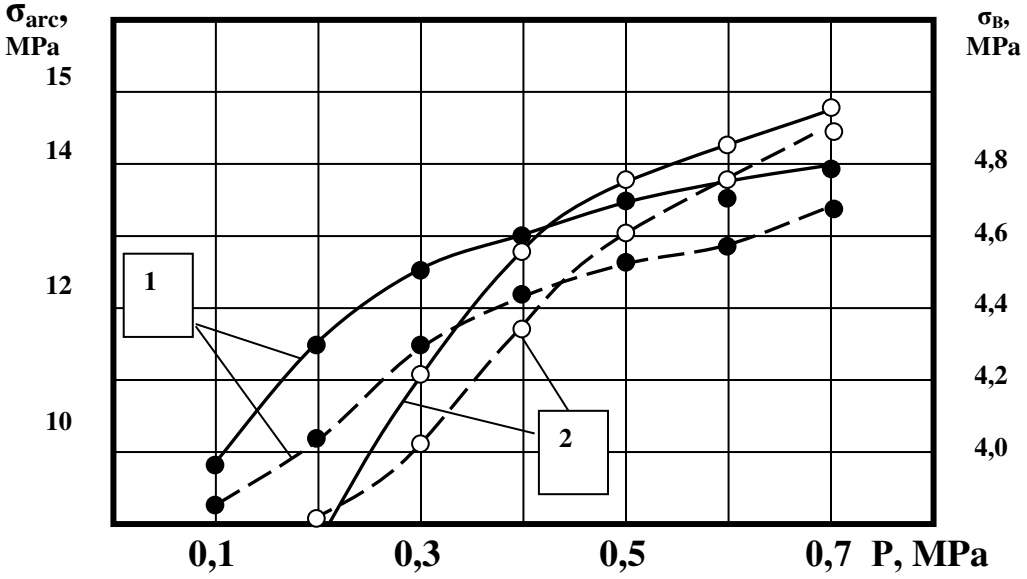

1 – K0315 70%+K02 30%, 2 – 1K02 70%+1K016 30%; solid line σ_p; dashed line σ_{arc}

Fig.11 – Various fraction sands effect on the mixture strength

Experimental determining the relationship between the time of the mixture holding on the heated plate (250 °C) and the shell thickness at various degrees of pressure shows that significant increasing the shell thickness does not occur. After P = 0.5 MPa, there is some increase in the shell thickness. Thus, there is no essential effect of pressure on the mold thickness.

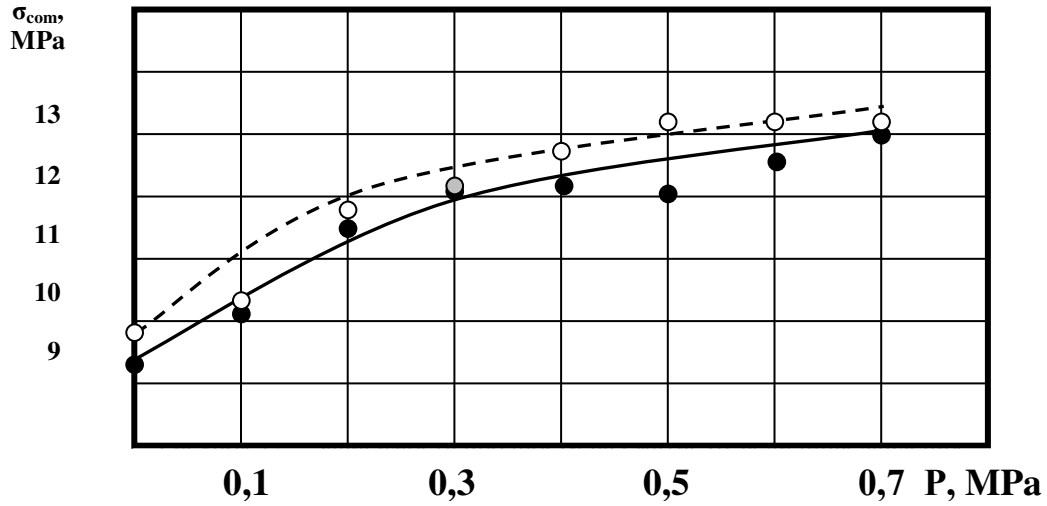

Fig. 12 – Dependence between the time of holding the mixture on the heated plate (250 ^{0}C) and the shell thickness under various degrees of pressure

Experimental determining the dependence of strength and density of the shell on the temperature of the model plate shows that with increasing the heating value of the model plate, the shell strength increases. However, as it is known from other experiments, significant increasing the temperature (above 400 °C) leads to burnout of the binder and, consequently, to the mold weakening. The composition of the mixture is as follows: sand 1K0315 70% + 1K02 30%, pulverbakelite 7%. The time of holding on the plate is 30 seconds. The data of this series of experiments are reflected in the graph (Figure 13).

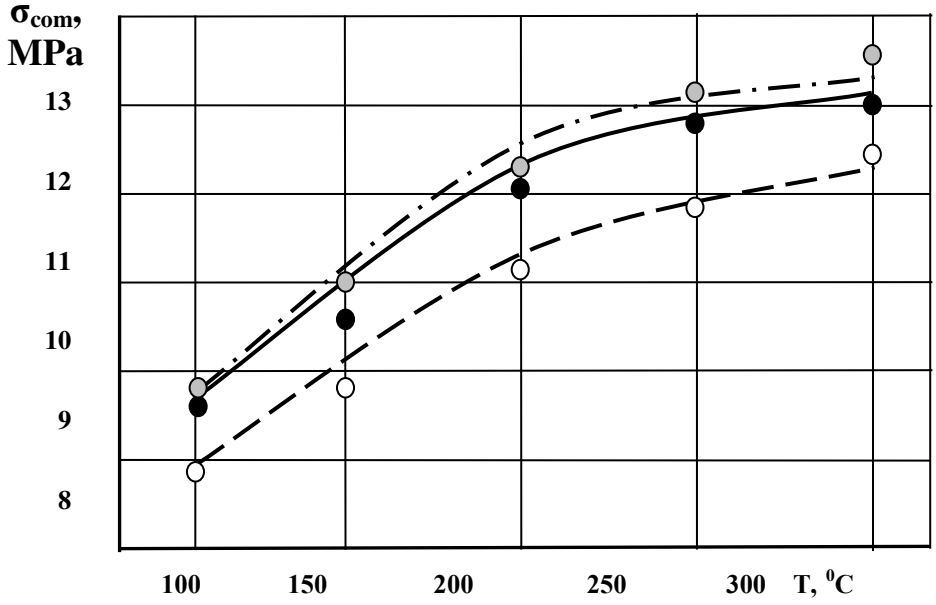

dashed-and-dotted line is 0.4 MPa; solid line is 0.3 MPa; dashed line is 0.2 MPa

Fig. 13 – Compressive strength dependence on the heating temperature in the course of mold shaping at various loads

The feasibility and optimal moment of some pressure increase in the course of shaping was determined in a series of experiments. The time of holding the mixture under pressure is 30 seconds. The initial pressure used is 0.2 MPa. The increase occurred at various intervals. The results of the experiments are presented in Figure 14. It is obvious

that the moment of increasing pressure is important. It is rational to do this at the beginning of shaping (after 10...15 seconds). Increasing the load in the final shaping is not advisable, moreover, it reduces strength as a result of breaking the structure of an almost shaped shell mold (squeezing sand grains from resin). Moreover, the more ΔP in the later stages of the shell shaping, the greater the extent of the mixture softening.

Based on the studies carried out, a molding machine and technology for manufacturing shell molds for heating equipment castings have been developed, tested in industrial conditions and proposed for use.

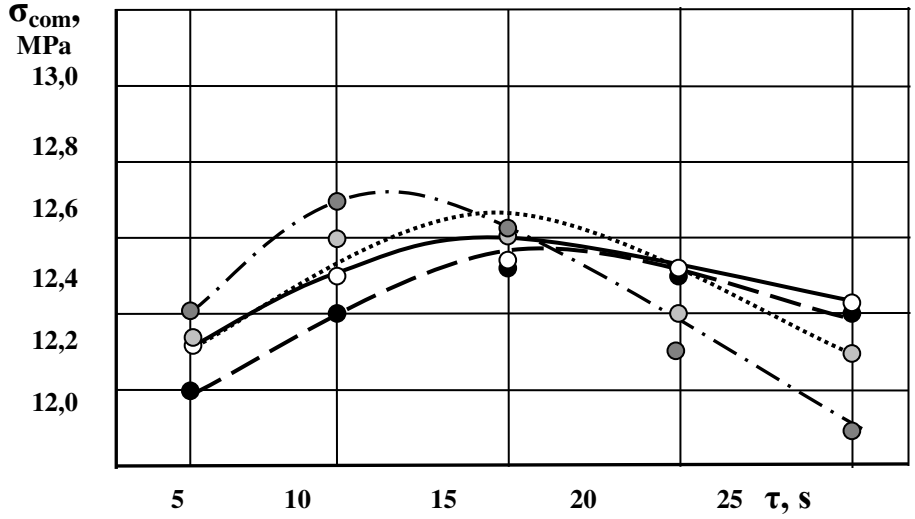

dashed-and-dotted line is ΔP=0.08 MPa; dotted line is ΔP=0.06 MPa;

solid line is ΔP=0.04 MPa; dashed line is ΔP=0.02 MPa

Fig. 14 – Compressive strength dependence on the moment of increasing static pressure on the disperse mixture

3. Conclusions

1. It has been established that the applying a load (0.18 - 0.22 MPa) during the process of the sand-resin mixture hardening significantly increases the purity of the inner surface of the mold, increases its mechanical properties (strength) and density, and reduces the amount of burns on the castings.

2. It has been found that the optimum pressure to obtain a dense and durable shell is the pressure on the mixture, consisting of the main and additional loads. The main load on the mixture is in the range of 0.18-0.22 MPa. Increasing the load in the process of the shell molding to 0.25 - 0.30 MPa increases the tensile strength of the sand-resin mold by 0.3-0.4 MPa.

3. A methodhas been proposed for removing harmful volatile substances and fine fraction dust emitted during manufacturing sand-resin molds by concentrating them in the cavity of the press plate with further centralized removal of harmful substances from the workplace by suction.

4. Using the proven technology with the use of static load for manufacturing molds for heating equipment castings allows reducing the castings reject and their metal intensity by reducing the wall thickness and improving the surface cleanliness (R_Z55-60). The resulting molds have uniform density and thickness of the shell (8-10 mm), and clearly reproduce the configuration of the model.

5. The developed method of manufacturing castings of heating radiators is acceptable for use in industrial conditions, it does not require high costs, reduces the number of reject and the cost of operations such as stripping, machining. This contributes to obtaining competitive products.

References

[1] Yu L., Xudong W., Yi S. Research on a new detection method of slab surface crack in mold during continuous casting //Metallurgical Research &Technology, 1 (108), 2018. - p. 321-329.

[2] Hiba B., Farida A., Delphine T. Thermomechanical behavior of resin bonded foundry sand cores during casting //Journal of Materials Processing Technology, 246 (8), 2017. - p. 30-41.

[3] Lei R., Lifeng Z., Qiangqiang W. Measurements of surface velocity and level fluctuation in an actual continuous wide slab casting mold //Metallurgical Research &Technology, 1 (102), 2018. – p. 282-287.

[4] Kmita, A., Fischer C., Hodor K. Thermal decomposition of foundry resins: A determination of organic products by thermogravimetry-gas chromatography-mass spectrometry (TG-GC-MS). Arabian Journal of Chemistry, 11(3), 2018. - p. 380-387.

[5] Illarionov I.E., Pestrikov V.F., Strelnikov I.A., Gartfelder V.A., Korolev A.V. Special types of casting //Cheboksary, 2015.

[6] Pastukhov A.G., Minasyan A.G., Sharaya O.A. Assessment of the stress-strain state of the press-mill chopper segment // Tekhnologiya Mashinostroeniya, №3, 2016. - p. 43-46.

[7] Gini E.Ch., Zarubin A.M., Rybkin V.A. Foundry technology. Special types of casting. - M.: Mashinostroenie, 2008. - 352 p.

[8] Zymankowska-Kumon S. Determination of the Content of the Phenol by the Pyrolysis Gas Chromatography-Mass Spectrometry Method //Archives of foundry engineering, No. 4, Vol. 18, 2018. - p. 83-86.

[9] Volkov D.A., Volkov A.D., Efimenko A.V. Shell casting and its versatility in small-scale and serial production //Liteyshik Rossii, № 4, 2016. - p. 26-30.

[10] Diaz Pace D.M., Miguel R.E., Di Rocco H.O. Blow-down laser spectroscopy. Free-laser-induced breakdown spectroscopy. //B-atomic spectroscopy, No. 5, Vol. 131, 2017. - p. 58-65.

[11] Vertsyukh, S.S., Znamensky, L.G., Ivochkina, O.V. Technology of casting into shell ceramic molds with the use of aluminoborophosphate concentrate. //Bulletin of South Ural State University. Series: Metallurgy, №253, 2011. - p.45-47.

[12] Volkov, D., Volkov, A.D., Efimenko A.V. Casting into small-scale and serial production. Foundryman of Russia, № 4, 2016. – p. 26-30.

[13] Kulikov V.Yu., Issagulov A.Z., Eremin E.N., Kovaleva T.V. Increasing the uniformity of density and increasing the strength of the shell mold. Foundry production. 2018. № 3. S. 27-29.5.

[14] Kvon Sv.S., Kulikov V.Yu., Filippova T.S.; Omarova A.E. Using high-chromium iron as material for production of the equipping components of mine shafts //Metalurgija, 55 (2), 2016. – p. 206-208.

[15] Kovalyov P.V., Ryaboshuk S.V., Issagulov A.Z., Kulikov V.Yu., Kvon Sv.S., Chsherbakova, Y.P., Sultamurat G.I., Jironkin, M.V. Improving production technology of tube steel grades in converter process //Metalurgija, 55(4), 2016. - p.715-718.

[16] Issagulov, A.Z., Kvon, Sv.S., Kulikov V.Y. Studying microstructure of heat resistant steel deoxidized by barium ferrosilicon. Metalurgija, №. 3, Vol. 55, 2016. - p. 388-390.

Control of Functionally Connected Surfaces of the Basic Details of Metal-Cutting Machines

Sherov K.T., Zharkevich O.M., Karsakova N.Zh.,
Okimbayeva A.E., Imasheva K.I.
Karaganda State Technical University, Kazakhstan

Abstract. The article deals with the control of V-shaped functionally connected surfaces. It gives classification of parts with surfaces having functionally related dimensions. Types of functionally connected surfaces of body parts and beds of machine tools are shown.
The article analyzes the design of special templates currently used to control the accuracy of locating the interrelated surfaces of the frame and the basic parts of machine tools. It was revealed that special templates and other existing universal means of angular dimensions control do not allow determining the magnitudes of angles with high accuracy. The limit of their measurements is 3' to 1° 55' that cannot meet the requirements for measurement accuracy in the machine-tool production. To solve this problem, a device has been developed for monitoring the inclination angle of the prism side surface of the lathe machine guide frame.

Keywords. Functionally connected surfaces, machine guides, V-shaped surface, body, tailstock plate, support, template.

1. Introducrion

One of the directions of modern science and technology development is improvement of advanced technologies widely used in production. Machine-tool manufacturing is an important aspect of mechanical engineering and one of the most labor-intensive industries [1].

Development of mechanical engineering in recent years has led to a focus on machining of functionally connected surfaces (FCS). In practice, more and more attention is paid to creation of methods, technological processes, tools, measurers, etc., that would decrease complexity of machining and assembly of parts and connections FCSs [2, 3]. Such surfaces in machine tools are guiding beds and supports. Phenomena that manifest themselves at the joints of V-shaped and flat guide machines, significantly affect the machining accuracy, vibration resistance of machine components and the quality of parts surface [4].

2. Results and discuss

FCS include surfaces of mobile and stationary joints, when the pairing is done simultaneously on several surfaces, and the accuracy of their pairing is determined by the contact standards [5]. Table 1 shows the classes of parts with FCS [4]. For some parts, such as gears, splined shafts, threaded surfaces and others, there are standards that regulate the FCS interconnection.

Table 1 - Classification of parts with surfaces that have functionally related dimensions

No. serial	Name of parts	Surfaces with FCS	Note
1	Gear wheels	Ring gear	GOST 1643-81 and others.
2	Slotted parts	Slotted surfaces	GOST 1139-80 and others.
3	Turnstiles	Ring gear	———
4	Threads and screws	Screw surfaces	GOST 16093-81 and others.
5	Body parts	Flat and V – shaped flat surfaces	———
6	Body parts	Dovetail surfaces	———
7	Bodies	Flat and V – shaped flat surfaces	———
8	Other details	Rack, lock and other surfaces	———

Currently, the relationship of the surfaces dimensions and positions is normalized not for all parts. These parts include body parts and bodies that have V-shaped surfaces and the planes related to them. Apparently, this is due to the large variety of FCSs and the complexity of dimensions technological support control.

From Table 1, it is clear that there is a great variety of details with FCS. Moreover, the surface may have a certain regular profile, for example, in the gear wheels they are evolvent, Novikov, arched profile, and etc. In other cases, these may be flat surfaces, for example, on splined shafts with a straight profile, or screw surfaces on threads, driving screws, etc. According to expert estimates [6-14], among the large variety of FCS, the problem remains with the provision of dimensional connections, processing technology and control of V-shaped surfaces and associated flat surfaces of machine tool parts.

On all machine tools, there are FCSs that are in contact with each other.

Figure 1 shows the types of FCS of body parts and bodies of machine tools.

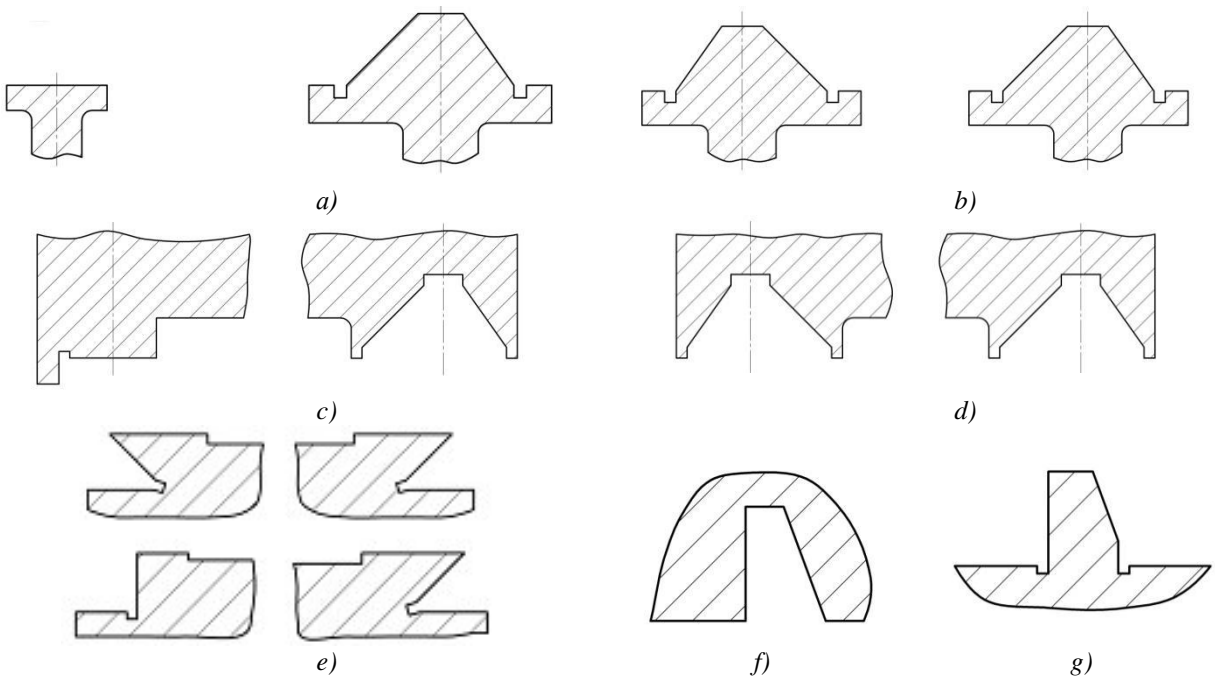

a) surface of average machines guide; b) surface of the guides of large machines; c) surface of the support guide of medium-sized machines; d) surface of support guide of large machines; e) carriage surface; e) surface of body guide of the tailstock; g) surface of tailstock plate guide

Fig. 1 - Types of FCS of body parts and bodies of machine tools

Figure 2 shows photographs of basic parts of lathes with FCS.

a) b)

a) tailstock (1) and tailstock plate (2); b) body

Fig. 2 - Basic parts of lathes with FCS

In the machine tool industry, the method of fitting by scrubbing the mating parts surfaces is widely spread. This method turned out to be the most acceptable due to the fact that the mating part, surfaces of which are scraped, is produced with very large tolerances and, consequently, with large allowances for machining.

Figure 3 shows the template for the manufacture of the body guide of NT-250I machine for the supports.

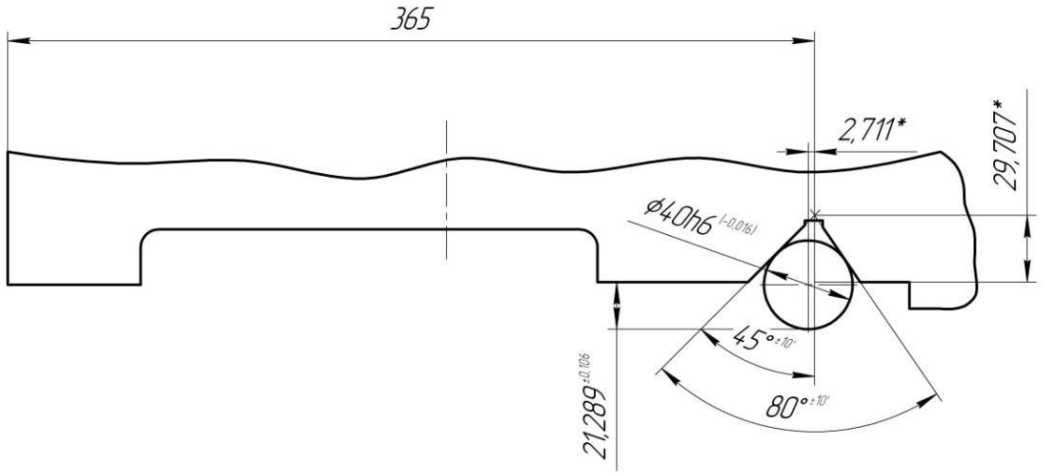

Fig. 3 - Template for the manufacture of the body guide of NT-250I machine for the supports

Figure 4 shows a sketch and a photograph of a template for the manufacture of body guides for NT-250I machine for the tailstock plate

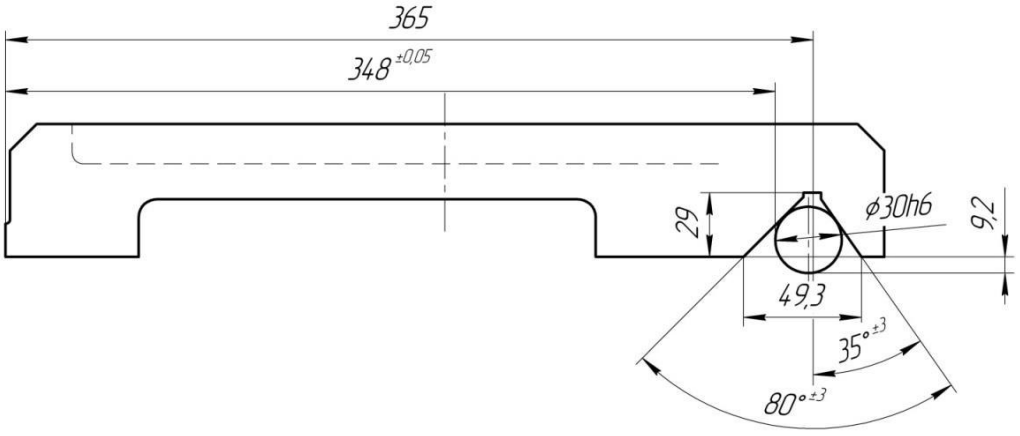

a)

b)

a) sketch of the template; b) photo of the template

Fig. 4 - Template for the manufacture of the body guide of NT-250I machine for the tailstock plate

Figure 1a shows the contours of the body guides in contact with the support of the NT-250I lathe. As a rule, location of body guide FCS with the help of angular dimensions is not specified. This is due to the fact that the body guides of the machine are such surfaces, where the mating parts surfaces are fitted - the support and the tailstock plate. To reduce to a more abbreviated terminology, we will call surfaces along which other surfaces are fitted, base surfaces or parts with base surfaces.

Dimensions and angular locations of the base surfaces are maintained with the help of special templates. Figure 3 shows a template for controlling the accuracy of the body interconnected surfaces location during their manufacture.

Moreover, the template in Figure 3 is designed to control the base surfaces for the supports of NT-250I machine. The base surfaces of NT-250I machine body are machined by final grinding on a longitudinal grinding machine. Since the body base surfaces are machined by checking with templates on the “clearance”, we can assume that the accuracy of the machine guides corresponds to the dimensional accuracy of the template.

Figure 3 also shows surfaces in contact with the body and dimensions between the functionally connected planes of the template for controlling the NT-250I machine guides. It is recommended to control the size of the template using a proof bar.

In the drawing of the template for controlling the accuracy of manufacturing the body guide of NT-250I machine for the supports, the following dimensions are shown:

- Ø40h6 is diameter of the proof bar;
- 29.707 * is distance from the top of the V-shaped surface to the plane of contact with the machine guides (size for the proof bar);
- 21.289±0.106 is the distance from the generating proof bar to the plane of contact with the guides of the machine;
- 80 ° ± 10’ is the angle of the template V-shaped surface;
- 45 ° ± 10’ is a part of the angle of the template V-shaped surface.

Such an arrangement of dimensions between the FCS is often used on the parts of machine tools.

From Figure 3 it can be seen that the total angle of the V-shaped surface at 80 ° is divided by nominal value into two unequal parts 45 ° and 35 ° relative to the perpendicular to the contact plane of the machine guides and the V-shaped surface passing through the top.

A device for monitoring the inclination angle of the lateral plane [15] has been proposed to control the FCS of the body guides of the lathes such as 1K62, NT - 250I and others with V-shaped prismatic projections.

Known devices of the type of template for controlling the position of the prismatic guide sides with respect to the plane of the lathe guide [16].

The disadvantage of the templates is their low accuracy in measuring the inclination angle of the side plane of the prismatic guide to the plane of the machine body guide due to the relatively low accuracy of manufacturing the corners of the template. The manufacturing errors of the inclination angles of the template planes are within ± 3'.

To control the inclination angle of the side plane of the prismatic guide to the plane of the body guide of the lathe, a vernier protractor can be used [17].

The disadvantage of the vernier protractor is their low accuracy in measuring the inclination angle of the side plane of the prismatic guide to the plane of the machine body guide due to the relatively low limit of the protractor measuring scale. The scale value of the vernier goniometer, depending on the model, ranges from 58’ to 1º55' and, as a rule, does not exceed 5'.

Figure 5 shows a device for monitoring the inclination angle of the prism side surface of the guide frame.

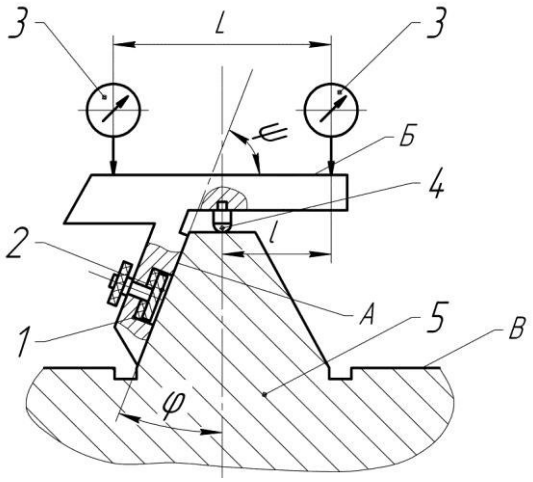

1 - case; 2 - magnet; 3 - dial indicator; 4 - support; 5 - body; A - controlled side of the prism; Б - control plane of the device; B - the plane of the guide frame; L is the distance that the dial indicator moves, φ is the prism controlled angle, I - I is the prism axis, ψ is the angle between planes A and Б.

Fig. 5 - Device for monitoring the inclination angle of the prism side surface of the guide frame

When measuring the inclination angle of the side surface of the body prism, the problem is to improve accuracy of measuring the inclination angle of the side plane of the prismatic guide to the plane of the machine body guide. This goal is proposed to achieve by measuring the inclination angle of the side plane of the prismatic guide to the plane of the machine body guide by the deviation from parallelism of the control plane on the device to the plane of the machine body guide by the formula:

$$tg\beta = \frac{u_1 - u_2}{L}. \quad (1)$$

where u_1 and u_2 are reading of the dial indicator in two relative to the device positions; L is distance between measurement points on the control plane.

Figure 6 shows the actual position of the control plane of device Б, depending on the actual position of the side plane A of the prismatic machine body guide.

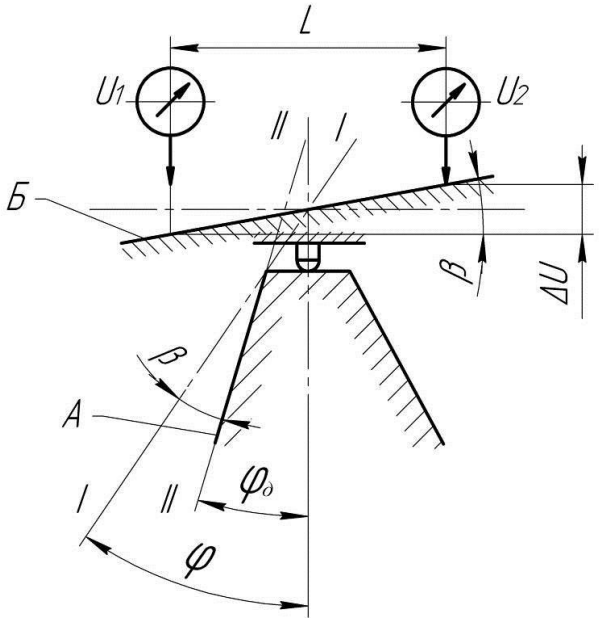

I - I is theoretical position of the side plane of the prism; II - II is the actual position of the side plane of the prism; β is the angle equal to the deviation of the actual angle $\varphi_д$ from the controlled angle φ; u1 and u2 are readings of indicator 3 in two relative positions.

Fig. 6 - Diagram of the actual position of the device control plane relative to its theoretical position

The inclination angle of the side plane of the prismatic machine body guide is controlled in the following sequence. The device case 1 is installed on the prismatic body guide 5 of the machine. Using a magnet 2 and two supports 4, a stable position of the device is provided on the body guides. The magnet takes the device to the guides of the machine.

The control sequence is shown in Figure 6. The dial indicator 3 moves parallel to the plane of the body guide B at a distance *L*. In case when the planes Б and B are not parallel, the dial indicator will show the deviation from parallelism Δu, determined by the difference in readings u1 and u2 by the formula:

$$\Delta u = u_1 - u_2 \quad (2)$$

The deviation Δu will be caused by the deviation of the actual angle φд from the controlled angle φ, the value of which is determined by the formula:

$$\beta = arctg\frac{\Delta u}{L}. \quad (3)$$

The use of the device will improve accuracy of angle φ measuring.

As an example, let's control the prism angle for 1K62 medium lathes. For these machines, it can be constructively assumed that L = 100 mm. When controlling the angle φ with a dial indicator with a graduation price of 0.001 mm, the error Δu = 0.001 mm presents when the angle φ deviates from β = 2.08 ".

The value of 2.08" characterizes the accuracy of measuring the inclination angle of the side plane of the guide to the plane of the guide machine, which is much higher than the requirements for the prism angle values .

Conclusions

1. The results of the study showed that the fundamentals of ensuring accuracy and quality of machining functionally related surfaces of machine parts, and in particular V-shaped and flat surfaces, are not sufficiently

highlighted in the literature. Uniform rules for assessing accuracy of interconnected dimensions have not been developed and metrological assurance of the accuracy of controling V-shaped and flat interconnected surfaces has not been developed.

2. Existing universal means of controlling angular dimensions, for example, templates, vernier protractors do not allow for determining the angles with high accuracy. The limit of their measurements is 3’ to 1° 55’ that can not meet the requirements for measurement accuracy in the machine-tool production.

3. A device has been developed to control the angle of inclination of the side surface of the guide prism of the machine body with increased accuracy ranging 2” to 5", which greatly exceeds the accuracy of existing universal measuring instruments.

The use of the device for controling inclination angle of the side plane of the prismatic lathe body guide [15] allowed the following advantages to be realized:

- to significantly improve the accuracy of measuring the inclination angles of the side planes of prismatic guides of machines to the plane of the body guides;
- to increase the requirements for the accuracy of angles in the drawings of parts;
- to reduce the complexity of finishing operations of mating planes machining.

References

[1] Koganov I.A., Kiselev V.N., Yamnikov A.S. Tochnost obrabotki na metallorezhushchikh stankakh: Uchebnoye posobiye / TulGU. Tula, 1996. - 132 p.

[2] Sherov K.T., Alikulov D.E. Control ruler for angles between planes of V-shaped guides //Measurement Techniques - New York, Volume 55, Issue 4, 2012. - p. 23 - 29

[3] Sherov K.T., Buzauova T.M., Karsakova N.G., Gabdysalyk R. Control’s accuracy improvement and reduction of labor content in adapting of ways of metalcutting tools / News of the Academy of Sciences of the Republic of Kazakhstan, Kazakh national research technical university named after K.I. Satpayev. Series of Geology and technical sciences, №6 (432), 2018. – P.170-179.

[4] Sherov K.T. Tekhnologiya sborki napravlyayushchikh metallorezhushchikh stankov [Assembly Technology for Metal Cutting Machine Guides] (monograph). - Karaganda: KSTU Publishing House, 2012. – 125 p.

[5] Koganov I.A., Nikiforov A.P., Sotova B.I., Gerlein M.O. Razmernyy analiz tekhnologicheskikh protsessov [Dimensional Analysis of Technological Processes]. - Tula: TulGU Publishing House, 1998. - 109 p.

[6] Suslov A.G.. Erokhin V.V.. Govorov I.V. Parametry kachestva funktsionalnykh poverkhnostey prizm [Quality Parameters of Prism Functional Surfaces] // Reference Book. Inzhenernyy zhurnal, №6, 2008. - P. 35-42.

[7] Yakobson M.O. Tekhnologiya stankostroyeniya [Machine Tool Technology]. - M.: Mashinostroyeniye, 1966. - 475 p.

[8] Fedosseyev D.N. Kachestvo sborochnykh operatsiy [Quality of Assembly Operations]. - L.: Mashinostroyeniye, 1971. - 248 p.

[9] Sherov K.T. Skhemy kontrolya i vzaimosvyaz parametrov prizmy [Control Diagrams and Interconnection of Prism Parameters]/ Vestnik Kazakhskoy akademii transporta i kommunikatsiy im. M. Tynyshpayeva.- Almaty: Pub.house of KazATK, No.6 (73), 2011. – p .234-238.

[10] Sborka izdeliy mashinostroyeniya [Assembly of Engineering Products]: Reference Book. V. 1/ Ed. V.S. Korsakov and V.K. Zamyatin. M.: Mashinostroyeniye, 1983. - 480 p.

[11] Dalsky A.M., Vassilyev A.S., Kondakov A.I. Tekhnologicheskoye nasledovaniye i napravlennoye formirovaniye ekspluatatsionnykh svoystv izdeliy mashinostroyeniya [Technological Inheritance and Directional Formation of Operational Properties of Engineering Products] // Izvestiya vuzov. Mashinostroyeniye. №10, 1996. - P. 70-76.

[12] Novikov M.P. Osnovy tekhnologii sborki mashin i mekhanizmov [Basics of Machines And Mechanisms Assembly Technology]. - M.: Mashinostroyeniye, 1980. - 592 p.

[13] Voskressenskiy Ye.A., Kopanyev V.V. Razrabotka iskhodnykh dannykh dlya optimizirovannogo podbora na sborku detaley. obrazuyushchikh pri soyedinenii odnu mnogozvennuyu razmernuyu tsep [Development of Initial Data for Optimized Selection for Assembling Parts Forming One Multilink Dimensional Chain When Connected] // Research in the field of machining and assembly technology: Collection of scientific papers TulPI. Tula, 1982.- P. 6-15.

[14] Konstruktorsko–tekhnologicheskoye obespecheniye kachestva detaley mashin [Design and Technological Provision of Machine Parts Quality]. / V.P. Ponmarev, A.S. Batov, A.V. Zakharov et al. - M.: Mashinostroyeniye, 1984. 184 p.

[15] Sherov K.T., Alikulov D.E. Ustroystvo dlya kontrolya ugla naklona bokovoy ploskosti prizmaticheskoy napravlyayushchey staniny tokarnogo stanka k ploskosti napravlyayushchikh stanka [Device for controlling the inclination angle of the side plane of the prismatic body guide of the lathe to the machine guides plane] // Conclusion on the issuance of an innovation patent of the Republic of Kazakhstan dated 30.11.2009 against application 2009/0578.1.

[16] Tekhnicheskiy kontrol v mashinostroyenii: Spravochnik proyektirovshchika [Technical Control in Mechanical Engineering: Designer's Handbook] / Endorsed by V.N. Chuprygin, A.D. Nikiforov. - M.: Mashinostroyeniye, 1987. - 512 p.

[17] Yakovlev V.N. Spravochnik slesarya montazhnika [Handbook for Fitter Installer]. 4th ed. reviewed and supplemented. - M.: Mashinostroyeniye, 1983. - 463 p.

Carbon Steel Modification when Exposed to Laser Radiation of Millisecond Duration

Lobankova O., Zykov I., Melnikov A.
Tomsk Polytechnic University, Russia

Abstract. The article considers the issues of surface hardening of structural carbon steel 45 by laser processing. As a result, the microstructure of laser irradiation areas, the microstructure of microhardness change in the hardened (one impulse) and unprocessed area, the microstructure of the laser irradiation area processed with five pulses, the microstructure of the tempered section of hardened steel and the microhardness change in the unprocessed, hardened and tempered areas were obtained. It was established that with an increase in the number of impulses per point, the processing depth increases by 1.5 times. It was found that an increase in the number of laser impulses to five significantly changes the structure of the processed area. The hardness of the treated steel decreases, but the viscosity of the material increases.

Keywords: laser exposure, microstructure, microhardness, dendrides, austenization

1. Introduction

Surface hardening of structural steels becomes a major factor in the conditions of progressive mechanization and automation of the manufacturing processes of machine parts. Responsible parts of modern machines and mechanisms are subjected to increased loads, which leads to rapid wear of parts. The durability of their use depends not only on the material from which the parts are made, but also on the method of their manufacture and on the preliminary processing of surfaces subjected to stresses. Traditional methods of surface processing have a number of limitations, i.e., high time and energy consumption, a complex heat processing mode, a wide area of heat impact, the absence of the solubility limit of excess phases and slow kinetics. In addition, some of the above methods are environmentally harmful and lead to environmental pollution [1]. There are many ways to modify the steels surface, but one of the most promising methods is laser processing. Compared to traditional methods of surface processing (gas-flame hardening, induction hardening, cementation, nitriding, nitrocarburizing, various hardfacing), laser surface modification has several advantages in solving tribological problems to ensure the operability of rubbing parts surfaces [1-3]. The indisputable advantages of laser hardening are the ability to process the local area and the rapid heating and cooling of the area subjected to processing [4, 5]. The surface of the heat processing using a laser beam is based on the features of self-hardening - it is rapidly cooled inward within the material without using a cooling medium, unlike conventional surface heat treatment.

In this regard, the goal of this research work is to study the physical and mechanical properties of the surface layer samples of structural carbon steel 45 after exposure to pulsed laser radiation and to identify the optimal parameters of heat processing leading to the formation of stable structures.

2. Material and Experiment's Method

For the study, structural carbon steel 45, widely used in industry, was selected. Steel samples 30 × 20 × 10 mm in size were prepared for laser processing in the annealed state.

A solid-state Nd: YAG laser operating in a impulsed mode with a radiation wavelength of 1.064 μm and an impulse duration of 12 ms and a power density of 23.4 kW / cm^2 was used as a laser radiation source. A rectangular impulse was used for the impact (the shape of the impulse allows to change the software of the laser complex) with a laser spot diameter of 0.35 mm. The surface processing of the sample was carried out with a frequency of one to five impulses at one point. The time interval between impulses was 3-5 seconds, which is due to the technological feature of the laser complex.

After laser processing, the samples were cut in such a way that after preparation for measuring the microhardness and studying the microstructure, the cut line passed through the middle of the laser exposure spot. To reveal the microstructure, polished sections were etched with a 4% solution of HNO_3 in ethanol. Along the depth of laser irradiation, microhardness was measured using a PMT-3 instrument under a load of 100 g. The microstructure of the samples was studied using an AxioObserver A1.m optical microscope (CarlZeiss (Germany) in AxioVision v.4.6 software.

3. Experiment's Results

During laser hardening of carbon steel in the impact area of the laser beam due to rapid heating and cooling, a very fine structure is formed, which cannot be etched with a standard etchant. The microstructure of the laser irradiation areas at various number of impulses is shown in Figure 1. With an increase in the number of impulses per point, the processing depth increases. It varies from 150-200 microns at one impulse to 400-450 microns at three impulses.

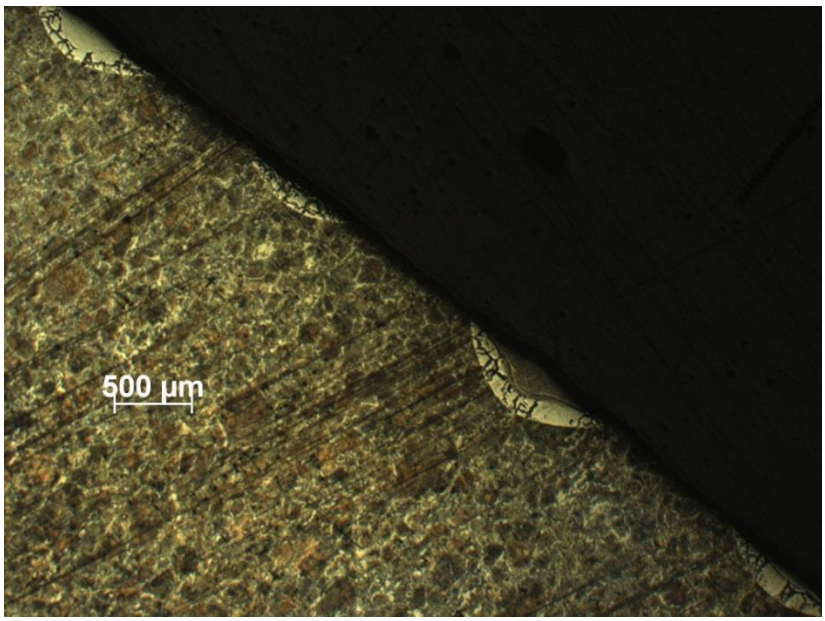

Fig. 1 - Microstructure of laser exposure areas

When considering the cross section of the processed area with laser radiation, several characteristic areas can be highlighted. In the center of the exposure spot is a fusion zone or a quenching zone from a liquid state. The structure of the processed area is not uniform. Against the background of a non-etching region, sections of the second phase are observed, which has a large affinity with the initial structure (ferrite). So, with a single impulse of irradiation, an inhomogeneous structure is observed over the entire area of laser exposure (Figure 1). The structure located in the center of the photograph). A further increase in impulses expands the non-etching area and reduces the area with a double phase (Figure 1).

Microhardness measurements showed that in the unprocessed area it is not large (Figure 2) and does not exceed 210 - 250 HV. As it moves toward the interface, the microhardness increases and is about 500 HV at the interface. In the field of laser exposure, microhardness has a maximum value that reaches 1080 HV. But there are areas of the second phase where the microhardness is much lower than the microhardness of the non-etching region surrounding these areas, where it has a value of 330 - 350 HV (Figure 2).

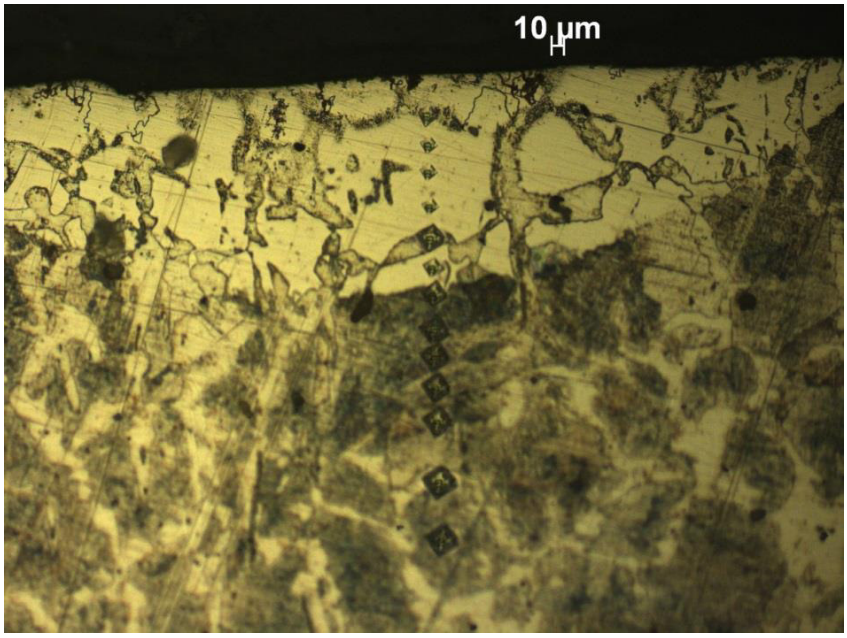

Fig. 2 - Microhardness change in the hardened (one impulse) and unprocessed area

Obviously, areas with lower microhardness are dendrites that grow perpendicular to the interface in the direction of heat removal deep into the sample. Or it's ferritic grains that did not have time to undergo a transformation, because the exposure time was not enough to complete the phase transition. This is evidenced by the fact that at the interface, the hardened and unprocessed zones, where the ferritic grains of the initial phase smoothly pass into the hardened zone.

Such heterogeneity of the structure is due to the fact that various stages of austenization take place during laser heating [6].

An increase in the number of impulses to five per one point substantially changes the structure of the processed zone. Figure 3 shows the microstructure of the zone processed with five pulses.

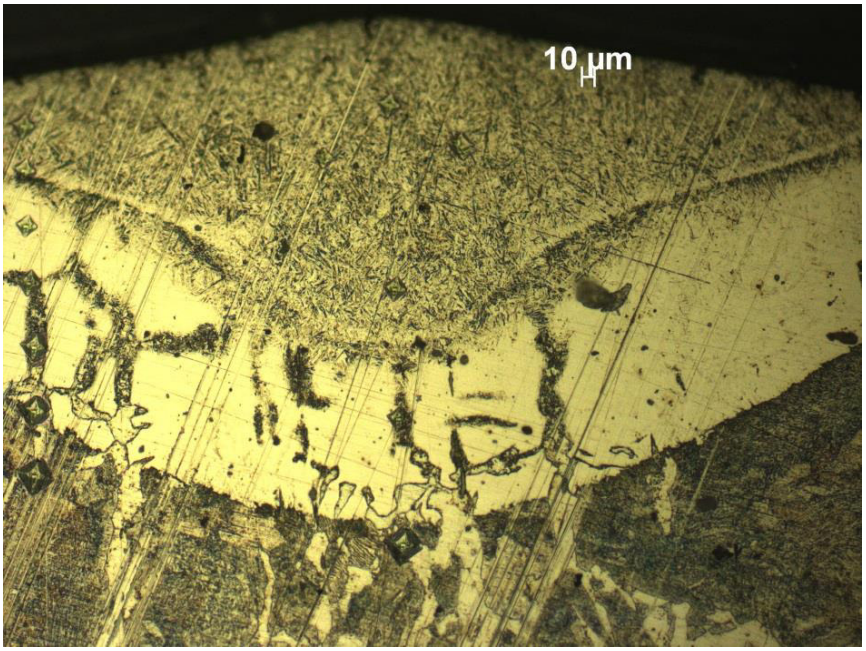

Fig.3 - The microstructure of the laser irradiated area processed with five impulses

It was shown that, along with the non-etched zone, another zone appears that has the structure of finely needle martensite, the microhardness of which is slightly lower and amounts to about 650 HV than the microhardness of the non-etched zone, where it has a hardness of 1080 HV (Figure 4). At this processing (five impulses), the surface layer of the area hardened from the liquid state is heated and a small needle-shaped martensite is formed. This structure has less hardness, but it increases the viscosity of the material.

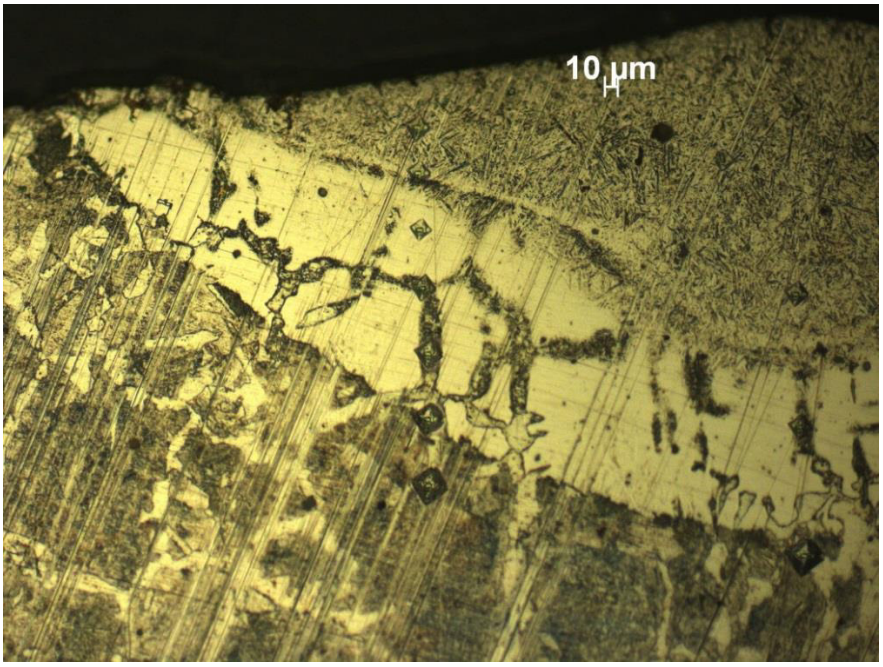

Fig. 4 - The microstructure of the tempered section of the hardened steel and the microhardness change on the unprocessed and hardened sections

4. Conclusion

The paper shows that laser processing of carbon structural steel with a single impulse leads to the formation of a structure with very high hardness.

The increase in the number of impulses per point, increases the processing depth from 150-200 microns with one pulse to 400-450 microns with three impulses.

Laser processing of steel 45 with five impulses enables to obtain the structure of finely needle martensite on the surface of the product, which, of course, somewhat reduces the hardness of the hardened layer, but at the same time increases the viscosity.

Laser processing in this mode enables hardening and tempering in one installation of the part, which reduces the complexity of the heat treatment process.

References

[1] Yaresko S.I. Analiz stoykosti i iznashivaniya tverdosplavnogo instrumenta posle lazernoy termoobrabotki //Izvestiya Samarskogo nauchnogo tsentra Rossiyskoy akademii nauk, № 1, T. 3, 2001. - P. 27–37.

[2] Magin D.Yu., Kostromin S.V. Issledovaniye struktury i svoystv vysokoprochnoy teplostoykoy stali posle obyemnoy termicheskoy obrabotki i lazernogo poverkhnostnogo uprochneniya //Trudy Nizhegorodskogo gosudarstvennogo tekhnicheskogo universiteta im. R.Ye. Alekseyeva, № 4, 2013. - P. 256–261.

[3] Sinyakov K.A. Vliyaniye skorosti nagreva na strukturu i svoystva instrumentalnykh staley //Instrument i tekhnologii, № 5, 2008. - P. 151–158.

[4] Grigoryants A.G. Osnovy lazernoy obrabotki materialov. - M.: Mashinostroyeniye, 1989. - 304 p.

[5] Ogin P.A. Struktura i svoystva zon perekrytiya pri lazernoy zakalke //Vektor nauki TGU. 2015. № 2 (32-2). - P. 130-135.

[6] Grigoryants A.G., Safonov A.N. Lazernaya tekhnika i tekhnologiya. Pod red. A.G.Grigoryants. – M.: Vyssh. shk., 1988. – 159 p.

Thermodynamic Simulation of Phase Equilibrium in the System CA - O – C

[1]Nurumgaliev A.Kh., [2]Toleuova A.R.
[1] Karaganda state industrial university, [2]Karaganda state technical university, Kazakhstan

Abstract. On the basis of the PC software "Terra" a complete thermodynamic simulation of phase equilibria of the ternary diagram of Ca-O- C in the temperature range 1573-2573 K and P = 0.1 MPa was conducted. In the article the results of a complete thermodynamic analysis (CTA) of high-temperature processes in the Ca - O – C system are given. The simulation results showed that the recovery process of the oxides CaO consists mainly of two stages: the first stage - the formation of calcium carbide; the second stage - the reduction of CaO with calcium carbide.

Keywords: thermodynamic simulation, high-temperature process, phase equilibrium, calcium carbide.

1. Introduction

Earlier, in the work [1 - 4] was shown that when using the method of complete thermodynamic analysis (CTA) with the addition of its thermodynamic diagram method of Gibbs concentration triangles construction is possible to construct the diagrams of phase equilibria in the ternary systems of the type Me-O-C. The effectiveness of this method was illustrated by examples of systems Fe-O-C, Si-O-C, Ge-O-C which are base for complex processing of alumina, silica and germanium ores of Kazakhstan. Investigation of private system Ca - O - C plays an important role in the analysis of complex multicomponent system Fe-Si-Ca-OC and production of calcium alloys.

2. Results and discussion

On the basis of the PC software "Terra" (with the addition of its thermodynamic-diagram method of concentration triangles «Triangle» constructing) complete thermodynamic simulation (CTS) of phase equilibria of the ternary diagram of Ca - O – C was conducted. The upper temperature limit is the melting point of working bodies, the lower - temperature of start interacting. P = 0.1 MPa. The PC-based method is the complete thermodynamic analysis (CTA), based on the principle of maximum entropy, and taking into account all the known properties of the reactants constituting thermodynamic system.

Composition of working bodies are shown in Table 1.

Table 1 - Composition of working bodies in diagram Ca – O – C

№	Component persantage, %			6 Ratio
	Si	O	C	7 O/C
1	10	10	80	0,125
2	20	70	10	7
3	10	60	30	2
4	42	48	10	4,8
5	20	50	30	1,67
6	70	20	10	2
7	20	40	40	1
8	40	30	30	1
9	70	10	20	0,5
10	50	10	40	0,25
11	10	40	50	0,8
12	24,5	55,5	20	2,78
13	38	45	17	2,65
14	32	38	30	1,27
15	28,5	33,5	38	0,88
16	80	12	8	1,5
17	61	22	17	1,29
18	56	32	12	2,67
19	95	2,5	2,5	1
20	20	20	60	0,33
21	10	80	10	8

On the sides of the diagram (Figure 1 and 2) compounds of stable phases are designated. On the side of the Ca - O there is one phase CaO, on the side of O - C: CO and CO_2, on the side of the Ca - C: SaC_2.

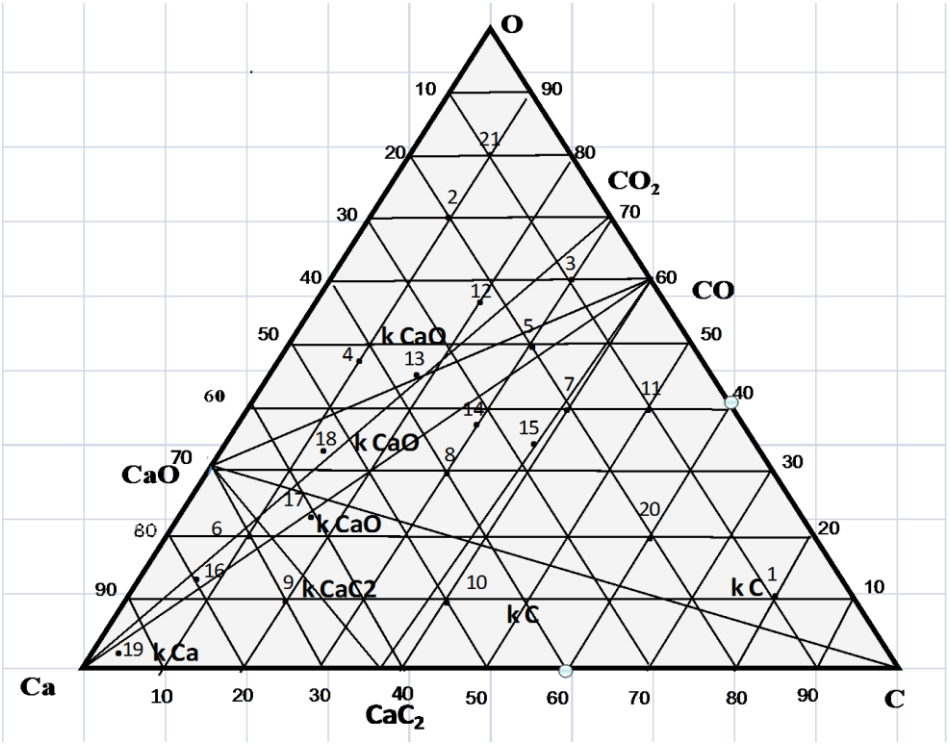

Fig. 1 - Diagram of Ca - O - C in the temperature range 1573-2073 K

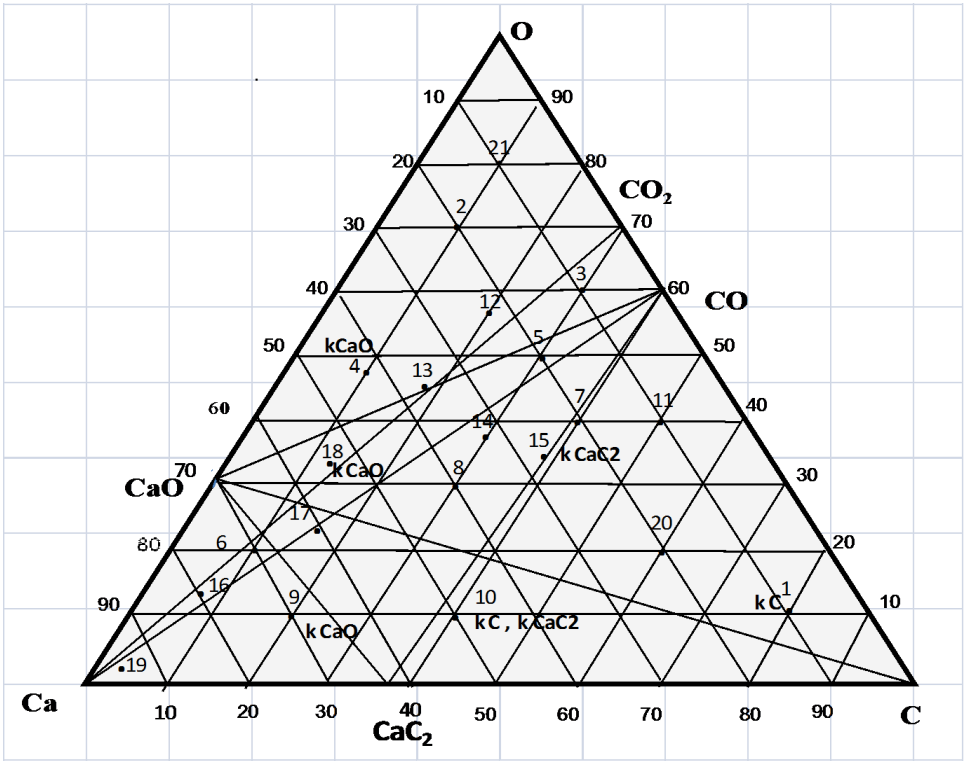

Fig. 2 - System Diagram Ca -O - C in the temperature range 2173-2573 K

For calculations working bodies are established and their composition diagram Ca - O – C are marked with points located on the lines connecting the following phases (Table 2, 3):

Table 2 - The composition of the system phases of Ca - O - C at 1573-1773K

Area	Phases	Compositions number
Δ CaO – O - CO	к CaO	т 2, 3, 4, 5, 12, 13, 21
Δ CaO – CO - C	к CaO, к C	т 1, 7, 8, 11, 14, 15, 18, 20
Δ CaO – C - Ca	к CaO, к CaC_2, к C, к Ca	т 6, 9, 10, 16, 17, 19

Table 3 - The composition of the system phases Ca – O – C at 1873-2173 K

Area	Phases	Composition numbers
Δ CaO – O - CO	к CaO	т 2, 3, 4, 5, 12, 13, 21
Δ CaO – CO - C	к CaO, к CaC_2, кС	т 1, 7, 8, 11, 14, 15, 18, 20
Δ CaO – CO – CaC_2	к CaO, кCaC_2, кС	т 7, 8, 10, 14, 15, 17, 18
Δ CaO – C - Ca	к CaO, кCaC_2, кС	т 6, 9, 10, 16, 17, 19

Based on the results of the calculations optimum compositions of points with maximum content of the condensed calcium have been identified.

Analysis of the calculation results of the equilibrium parameters for content with maximum calcium ranging to areas CaO - C - Ca, shown in Table 2 and 3 shows that the equilibrium phases are к Ca, кCaC_2.

Table 4 shows the compositions of the equilibrium phases for points 9, 16 and 19.

Table 4

The composition of the equilibrium phases

Phase, ml/kg	Temperature, K										
	2573	2473	2373	2273	2173	2073	1973	1873	1773	1673	1573
1	2	3	4	5	6	7	8	9	10	11	12
т. 9 Ca= 70 C = 20 O = 10											
кCaC_2	5,20	5,20	8,06	8,30	8,32	8,32	8,32	8,32	8,32	8,32	8,32
кCaO	-	-	5,72	6,19	6,25	6,25	6,25	6,25	6,25	6,25	6,25
кCa	-	-	-	-	-	-	-	-	-	2,89	2,89
т. 16 Si = 80 C = 12 O = 8											
кCaC_2	-	-	2,49	3,24	3,32	3,33	3,33	3,33	3,33	3,33	3,33
кCaO	0,84	0,84	5,83	7,32	7,47	7,48	7,50	7,50	7,50	7,50	7,50
кCa	-	-	-	-	-	-	-	-	9,13	9,13	9,13
т. 19 Ca = 95 C = 2,5 O = 2,5											
кCaC_2	0,26	0,26	0,26	0,83	1,01	1,04	1,04	1,04	1,04	1,04	1,04
кCaO	-	-	-	1,14	1,50	1,56	1,56	1,56	1,56	1,56	1,56
кCa	-	-	-	-	-	-	-	-	-	21,10	21,10

The complete graphs results of thermodynamic analysis (CTA) in the temperature range T = 1573 - 2573 K are shown in Figure 3.

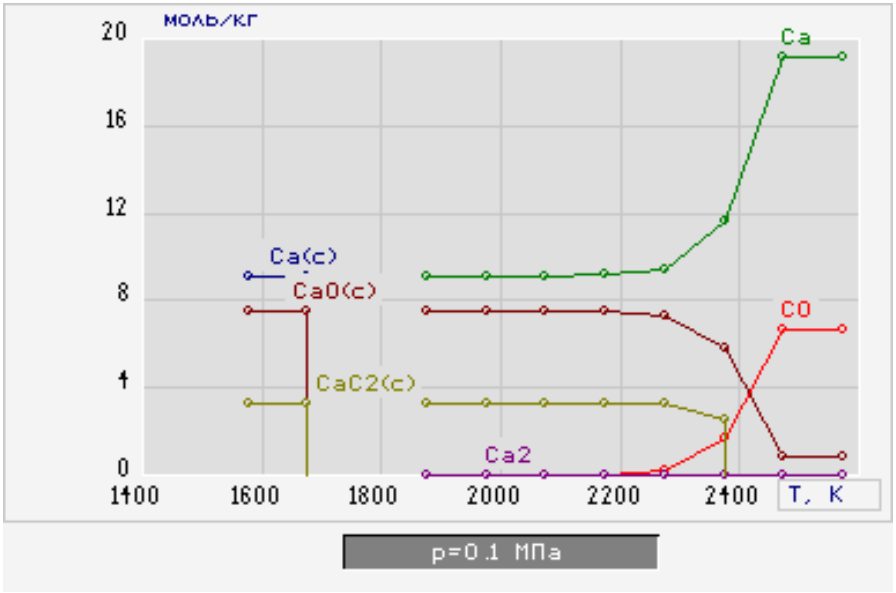

Fig.3 - System graph Ca - O - C in temperature range 1573-2573 K for point 16

With the help of the program «Triangle» the distribution of the composition of the condensed phase equilibrium at temperature 1573K is shown in Figure 4.

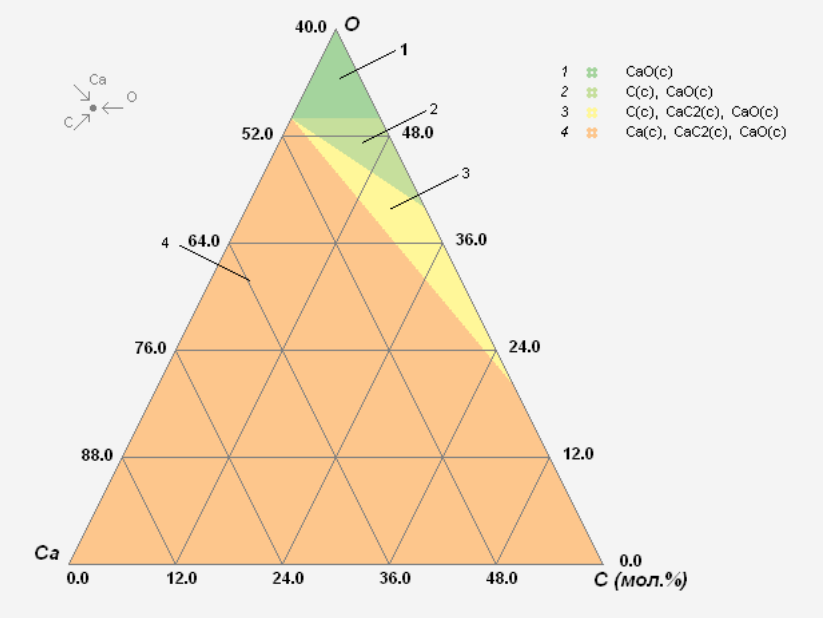

Fig. 4 - The composition distribution of condensed equilibrium phases at a temperature of 1573K

As seen from the data in the CaO - O – CO the basic and unique condensed phase is kCaO therefore there is no interaction between existing phases in this area and the region is monophasic. The remaining areas are isophase. Based on the results of CTA we write down the reaction of the initial phases in the entire temperature range.

There is no gas phase in the CaO- CaC_2-Ca at point 19 in the temperature range T = 1573 - 1673 K. The presence in the form of condensed phases kCaO, $kCaC_2$, kCa as the interaction products is observed. We write down the reaction with the material characteristics of the following temperatures:

1573 -1673 K 1773 K

Including CaO + C = 19 21,099 кCa + 1,5626 кCaO + 1,0407 $кCaC_2$ = 1,5626 кCaO +

2373-2573 K

1,0407 $кCaC_2$ + 21,057 Ca = 0,25944 $кCaC_2$ + 23,423 Ca + 1,5625 CO

It follows that as a result of chemical interaction act at T 1573 – 1673 K in the first stage condensed phases of calcium, carbide calcium and calcium oxide are formed. At higher temperature gaseous Ca and CO are formed.

Thus, the primary reductant for reaction during the interaction is calcium carbide carbon. The reaction is fully correspond to the conditions of the thermodynamic and phase equilibrium.

As a result metallic calcium is formed only in ΔSa – CaO – SaC_2.

Thus the result analysis of CTA and reactions on their base shows that the recovery of calcium consists essentially of two stages:

- the first stage - the formation of calcium carbide;
- the second stage - the restoration of CaO calcium carbide.

The products of the interaction in the selected temperature range, depending on the composition of the working bodies can be phase: $кCaC_2$, кCa, кCaO and their various relationships.

References

1.Simbinov R.D., Malyshev V.P. The thermodynamic and stoichiometric Exergic modeling of phase equilibria. Almaty: Gylym, 1999, p. 100.

2. Simbinov R.D. The thermodynamic and stoichiometric modeling of phase transformations in the system Fe - O - C // Reports National Academy of Sciences RK. Almaty, 2002, №1, p.42 – 50.

3. Simbinov R.D. Thermodynamic modeling of high-temperature processes in the system Ge-O-C // Tidings MES, NAS RK. Series chem. Almaty, 2002, №1, p. 87 – 91.

4. Nurumgaliev A.Kh., Bekkulina Ph.Zh., Zhankina A.K. Thermodynamic modeling of high-temperature processes in the SI - O - C // SCIENCE AND PEACE International Journal, № 4 (8), 2014, Band, p. 102-106.

5. Nurumgaliev A.Kh., Baisanov S.O., Dmitriev L.N. Involvement of coal waste from the Ekibastuz basin in the smelting of silicon-aluminum alloys. Karaganda, 1993, p.201

6. Nurumgaliev A.Kh., Baisanov S.O., Dmitriev L.N. Development of technology for smelting alloys based on silicon and aluminum from carbonaceous rocks of the Ekibastuz basin. Almaty:Gylym, 1993, p. 270